

3D SIMULATION OF EXTERNAL BEAM RADIOTHERAPY

Vom Fachbereich Informatik
der Technischen Universität Darmstadt



zur Erlangung des akademischen Grades eines
Doktor der Ingenieurwissenschaften (Dr.-Ing.)
genehmigte Dissertation
von

M.Sc. Grigorios Karangelis

aus Trikala, Griechenland

Referent: Prof. Dr. –Ing. José Luis Encarnação
Korreferent: Prof. Dr. –Ing. Georgios Sakas

Tag der Einreichung: 29 Oktober 2004
Tag der mündlichen Prüfung: 13 December 2004

Darmstaedter Dissertation - D17

Acknowledgments

Hereby, I show gratitude to all the persons who have involved and contributed directly or indirectly to my work and to this thesis.

I would like to express my deepest appreciation to my supervisor, Prof. José Luis Encarnação, for giving me the chance to share probably the most important part of my career in an ideal scientific environment, which he and his partners manage to build over years at FhG-IGD in Darmstadt. His guidance and support has been for me the best supplies to go accomplish this task.

Comprehensive thanks go to Prof. Georgios Sakas, for giving me the chance to visit Germany and to initiate here my career. His constant support on the preparation of this thesis, on scientific projects and on life matters have been by far the most valuable supplies for me all these years. The same valuable feelings I express for Prof. Nikolaos Zamboglou, the father of Exomio, for his extremely helpful scientific input during the project Exomio, offering an excellent clinical environment to develop our application. I would also like to thank him for his comments and suggestions on my work. I will never forget his motivation and emotional support on several issues. Further more I would like to thank the directors of Medintec GmbH, Ulrich Borman and Erik Van Hoft, for the financial support of the Exomio project. In addition special thanks goes to Prof. Dr. Dimos Baltas for his valuable support on different matters.

I feel deeply grateful to my formal director in Technical Institution of Athens for his encouragement on taking a big step in my life, Prof. Dr. Dionisis Cavouras. Further more I would thank all my colleagues and students in the department of Cognitive Computing and Medical Imaging, for providing me so much help all these years. Among them, I would express my special thanks to all persons involved in the Exomio project developments, and mostly to my old friend and colleague, Wenli Cai, for his support during my first years in Darmstadt. Analogous thanks I express to Stefan Volmer and Stefan Walter. My special thanks goes also to my IGD colleagues Min Wang, Evelyn Firle, Stefan Wersag and Wei Chen. Special thanks goes to the formal IGD visitor Eliana Vasquez Osorio, for the excellent scientific cooperation and brainstorming. Part of recognition goes to her Prof. Oscar Ruiz for an excellent cooperation during his visit.

My appreciative thanks goes to all colleagues in Medcom GmbH for their contribution during Exomio project, especially to Marcus Grimm and Roland Ohl. My Greek thanks I would like to offer to the Greek engineering group composed from Gianni Nomikos, Stelios Zimeras and Ilias Saxpazidis for the nice times we had together. Also, I like to express my thanks to all the other formal IGD members and students working or having worked in our InViVo family, including Michael Richtscheid, Stefan Großkopf, Jürgen Jäger, Michael Lahanas, Matthias Balwierz, Marian Wischkony, and Nicolas Weber.

Finally, I would like to thank the most precious people of my life; my family and especially my wife for her unlimited patience and support all these years.

Preface

Computer Graphics (CG) is the technology with which pictures – in the general sense (synthetic graphics as well as grayscale and color images) – are generated or acquired, managed, displayed, processed in an application-oriented manner by means of computers, and with which pictures are also correlated with non-graphical application data (From IGD - Computer Graphik TOPICS Magazine). The evolution of CG the last 30 years enabled important computer science and information technology trends to incorporate in many daily life aspects [Encar03]. As an example, although CG technology and medicine are two sciences very different to each other, excellent results for the patient diagnosis and treatment outcome can be achieved if both are combined, improving this way the quality of life.

In the last 25 years the introduction of the computers in medicine was mend to open new horizons for several medical applications. The evolution started using computers for complex and time-consuming calculations. This could involve the processing of large amount of data or the derivation of complex mathematical results. Beyond that assistance the greatest evolution in medical technologies was brought through medical imaging and applied computer graphics in medicine. The applications are several and can be separated into simple diagnostic procedures up to very complex treatment surgery. Although that medical imaging applications in radiation therapy can be separated into several categories and many of them require intensive calculations, imaging components are essential. The use of properly build technology allows nowadays non-expert computer users in medicine, usually medical oriented users, to administrate software applications and to contribute in the daily clinical outcome with much higher influence.

Most medical imaging application base their functionality on replacing the physical patient model with the digital data of the patient coming from any medical imaging modality. Medical imaging techniques offer unique capabilities on collecting digital data of the human body. Nowadays technical evolutions allow the generation of 3D data within a few moments. This is a fact for several imaging modalities. The 3D data set have a great benefit over conventional 2D images, especially in cases with complex anatomy or pathology. Clinical evaluations of current 3D techniques imaging have demonstrated their usefulness in both diagnostic and therapeutic applications. Computed tomography is the most common modality used in radiation oncology mostly due to the use of the HU and their relation with the electron densities of the tissues. Recent advances in the specific area are the helical CT and nowadays the volumetric helical CT scanner. These systems have the capability to generate CT volumes with high contrast, high resolution and low noise with in a few seconds.

Radiotherapy treatment is a very demanding cancer treatment process. The aim of the treatment is to cure or to limit the disease having as minimum as possible damage of healthy tissues, the process is composed from several steps that they are highly depended to each other in order to bring the wanted result. One could separate them into three deferent categories; the treatment planning and evaluation, the planning verification before and after treatment and finally the treatment itself. It is reasonable to think that a very precise planning of a treatment would be a failure if the patient positioning during treatment were wrong; and of course vice versa, an exact patient positioning during treatment would be useless as long as the planning process has been done incorrectly. To avoid any of the above cases to occur they must be evaluated using the appropriate verification tools and procedures, which also must be accurate and previously clinically established. Since a few years ago a big part of the above procedures use to take place with

several hardware components involved. Currently more and more procedures are going digitally and it has become a common aim for the oncology clinics to go filmless, which is a cost effective and productive solution.

The above, present the state of the art. This work is a contribution in the chain of the radiotherapy process from the medical software application point of view. The results of this work are focusing, to provide direct and indirect assistance to a group of patients suffering from cancer disease. In principle the digital patient data are used instead of the physical patient in order to perform the geometric planning. The results of this work involve the planning and partly the evaluation steps of the radiation therapy process.

Fully 3D definition of volumetric structures is a unique feature introduced from this thesis. Such functionality provides higher degree of freedom to the clinicians for investigating fully the 3D information of the digital volumes. Semi-automatic segmentation of the spine is an essential tool used delay for the extraction of the spine's volume in order to prevent its exposure on high dose levels. Main advantages of the methods are the increased efficiency and the improved time rates during volume segmentation.

An interesting part of this work is the compensation of breathing artifacts as they are recorded and reconstructed on the surfaces of the acquired computed tomography medical volumes. This kind of artifacts is a source for potential errors during treatment planning and treatment evaluation. In this work we present a method for eliminating these inaccuracies and thus improving the treatment outcome.

Volume rendering is the basis for a 3D-Simulation system. Thus interactive volume reconstruction of specific body regions is always an essential tool for such systems. In this work a unique method is presented that improves reconstruction of sensitive anatomical structures and requires the minimum possible user interaction. The results of the method are unique and revolutionary for radiation therapy planning.

Finally we address a very essential issue related with the treatment planning verification. Standard methods involve the use of quantitative and numerical statistics methods of the treatment dose distribution over the target volume and the segmented organs. In this work we present methods for the visualization of the dose distribution in relation to the standard patient anatomy and the segmented anatomical structures. The results provided are unique for the qualitative treatment plan evaluation.

The solutions provided have been hosted under the 3D simulator system called *Exomio*. *Exomio* aims to assist clinicians to improve the geometric planning of the patient treatment and to replace the conventional simulator system in the oncology clinics. Thus beyond the improvement of the clinical outcome and the reduced patient treatment administration bottle-neck, the clinics can reduce the patient treatment expenses using a cost effective software solution.

Frequently Used Abbreviations

1D, 2D, 3D	{one, two, three}-dimensional
3D-Sim	3D Simulation Software System
BEV	Beam's Eye View
BTF	Back-to-Front
CT	Computed Tomography
CTV	Clinical Target Volume
DICOM	Digital Imaging and Communications in Medicine
DVR	Direct Volume Rendering
DVH	Dose volume Histogram
DRR	Digital Reconstructed Radiography
GUI	Graphics User Interface
Exomio	3D simulation system
HU	Hounsfield Unit
InViVo	Interactive Visualizer of Volume Data
LN	Linear Interpolation
LiNAC	Linear Accelerator (External beam treatment unit)
LUT	Look Up Table
MIP	Maximum/Minimum Intensity Projection
MPR	Multiplanar Reconstruction - 2D image interpolated from 3D data
MRI	Magnetic Resonance Imaging
OEV	Observer's Eye View
PET	Positron Emission Tomography
Planning	Cancer Treatment Planning
PTV	Planning Target Volume
RTP	Radiotherapy Treatment Planning
RT	Radiotherapy Treatment
ROI	Region of Interest
Simulator	Radiotherapy Simulator Machine
SAD	Source to Axis Distance
SID	Source to Image detector Distance
SPECT	Single Photon Emission Computed Tomography

SR	Surface Rendering
SSD	Source to Skin Distance
TCP	Tumor Control Probability
TF	Transfer Function
TPS	Treatment Planning System
VOI	Volume Of Interest
VS	Virtual Simulator
VSS	Virtual Simulation System
voxel	Volume Element

Table of Contents

Chapter 1

Introduction	1
1.1 Introduction.....	1
1.2 The External Beam RT Process	1
1.2.1 Target Volume Determination	1
1.2.2 Treatment Planning.....	2
1.2.3 Treatment Verification.....	2
1.2.4 Treatment Delivery.....	2
1.3 Role of Simulation in RT process	3
1.3.1 The Conventional Simulator	3
1.3.2 The Virtual Simulator.....	4
1.4 Related Work	6
1.5 Challenges in 3D-Simulation	7
1.6 Summary and Contributions	8

Chapter 2

3D Virtual Simulation: System Concept.....	10
2.1 Introduction.....	10
2.2 The Treatment Simulator.....	11
2.2.1 Simulator's Gantry.....	13
2.2.1.1 Imaging Components.....	14
2.2.2 Simulator's Table and Table Top	15
2.3 3D-Simulator: System Concept	16
2.3.1 Volume Rendering: An essential part in 3D-Simulation systems	17
2.3.1.1 Transparent Modes.....	18
2.3.1.2 Surface Reconstruction.....	25
2.3.2 Radiation Beam Arrangement and Visualization	25
2.3.2.1 Polygon Scan Conversion	26
2.3.2.2 Projection of the Virtual Light Field.....	27
2.3.3 Room View.....	29
2.4 Summary.....	32

Chapter 3

Segmentation of Anatomical Structures.....	33
3.1 Introduction.....	33
3.2 Manual Definition of Structures.....	34
3.2.1 Volume Interpolation from Parallel & Non-Parallel Contours	37
3.2.1.1 Radial Basis Function Approximation.....	38
3.2.1.2 Prepare Constrains for 2D Input Contours	41
3.2.1.3 Surface Reconstruction from Parallel Contours.....	42
3.2.1.4 Non-Parallel Contours.....	45
3.3 Segmentation of Normal Tissues.....	48
3.4 Segmentation of the Spinal Canal	48
3.4.1 Definition of Starting Point.....	50
3.4.2 The Boundary-Tracking Algorithm.....	50
3.4.3 Tracing Conditions	52
3.4.4 Results.....	54
3.5 Summary	55

Chapter 4

Fast Smoothing of Superficial Respiration Artifacts in CT Volumes.....	56
4.1 Introduction.....	56
4.2 Related Work.....	57
4.3 Generation of Body Surface.....	59
4.3.1 Generation of Body Planar Contours.....	60
4.3.2 Sampling Rate Selection.....	62
4.4 Smoothing Filter	62
4.5 Surface Smoothing	64
4.5.1 Surface Signal Constrains.....	64
4.5.2 Control of Filter Iterations.....	64
4.6 Results	67
4.7 Summary.....	70

Chapter 5

Improved Volume Rendering of Thoracic CT-Volumes	71
5.1 Introduction.....	71
5.2 Related Work.....	71

5.3	Conventional Volume Rendering	74
5.4	Region Growing	77
5.5	Rendering & RG Results.....	78
5.5.1	Direct Surface Reconstruction.....	79
5.5.2	Integration to DRR Reconstruction.....	80
5.5.2.1	Direct DRR Reconstruction.....	81
5.5.2.2	DRR and Direct Surface Rendering Mixing	86
5.6	Integration into 3D Simulation.....	88
5.7	Summary	90
Chapter 6		
Efficient Visualization of Dose Distribution.....		93
6.1	Introduction.....	93
6.2	Related Work	95
6.3	Dose Volume Interpolation	97
6.3.1	Nearest Neighbour (NN)	98
6.3.2	Linear Data Interpolation.....	98
6.3.3	B-Spline Interpolation.....	100
6.4	Dose Volume Visualization	104
6.4.1	Merging VOIs and CT Volume	105
6.4.1.1	Intensity Intermixing Only	106
6.4.1.2	Intensity Intermixing with Z-buffer Depth Difference	107
6.4.2	Merging VOIs and Dose Volume	108
6.4.2.1	Inclusive Opacity (INCOP)	108
6.4.2.2	Dose Mapping on VOIs	110
6.4.2.3	3D Visualization of the DVH.....	111
6.4.3	Merging CT Volume and Dose Volume	114
6.4.3.1	Direct Dose Mapping.....	114
6.4.3.2	Selective and Inclusive Opacity.....	115
6.5	Summary	115
Chapter 7		
Summary.....		118
7.1	Segmentation of Anatomical Structures.....	118
7.2	Fast Smoothing of Superficial Respiration Artifacts in CT-Volumes.....	119

7.3	Improved Volume Rendering of Thoracic CT-Volumes.....	120
7.4	Efficient Treatment Dose Visualization in CT-Simulation	121
7.5	Future Directions	121
References		123

Table of Figures

Figure 1-1. RT clinical Routine and data workflow using conventional Simulator	2
Figure 1-2. Illustration of the conventional Simulator	3
Figure 1-3. RT clinical Routine and data workflow using 3D-Simulator	5
Figure 2-1. An industrial simulator type from Elekta.....	12
Figure 2-2. Hardware configuration of the digital radiotherapy simulator	13
Figure 2-3. Basic simulator components as defined from IEC 1217	14
Figure 2-4. Simulated collision.....	15
Figure 2-5. Definition of the real Simulator treatment field	16
Figure 2-6. Simple block diagram of the 3D-Simulation system of radiation therapy	18
Figure 2-7. Reconstruction of a CT chest volume using MIP	19
Figure 2-8. Attenuation of original ray energy I_0 to $I_{(s)}$ though a sequence of materials	20
Figure 2-9. DRR reconstruction of CT chest volume.....	22
Figure 2-10. Direct volume surface reconstruction	24
Figure 2-11. Simplified Z-depth estimation during polygon scan conversion.	27
Figure 2-12. Projection of treatment field with patient anatomy	28
Figure 2-13. Graphical representation of the conventional simulator environment	29
Figure 2-14. Indication of potential collisions during RT treatment.....	30
Figure 2-15. A representation of the 3D-Simulator (Exomio)	31
Figure 3-1. Illustration of CT slices using different windowing functions.....	35
Figure 3-2. Manual segmentation of the left lung region.....	35
Figure 3-3. 3D representation of RBFs used in this work	39
Figure 3-4. Extraction of normal constrains from the original contour.....	41
Figure 3-5. Contour tracing on a grid	43
Figure 3-6. Reconstruction of kidney surface from parallel contours	44
Figure 3-7. Contour samples defined according to trachea shape	44
Figure 3-8. A simple surface reconstruction example from orthogonal contours.....	45
Figure 3-9. Surface reconstruction of a femur.....	46
Figure 3-10. Definition of non-parallel contours on CT slices	47
Figure 3-11. Illustration of different spinal cord vertebrae as anatomical sketches.....	48
Figure 3-12. Discontinue spinal canal.....	49

Figure 3-13. Angular tracing of open vertebra boundaries.....	50
Figure 3-14. Spine boundary tracking of single slices.....	51
Figure 3-15. Difference between simple image thresholding (a) and gradient detection (b)	52
Figure 3-16. Wire loop display of the traced spine contours	52
Figure 3-17. Linear interpolation between key contours	53
Figure 3-18. Comparison of manual and computer traced spinal cord contours	54
Figure 4-1. Torso volume illustration with treatment field.....	57
Figure 4-2. Most left-Original volume data reconstructed with volume rendering	58
Figure 4-3. Deformation of an axial body contour during breathing	60
Figure 4-4. Angular sampling rate selection	62
Figure 4-5. The moving average filter and filtering examples	65
Figure 4-6. Comparison between interpolated and non-interpolated smoothed curves	66
Figure 4-7. Results of quantitative comparison between original and reformatted torso-contours	67
Figure 4-8. Comparison of contour smoothing results.....	68
Figure 4-9. Different surfaces smoothing examples	69
Figure 5-1. Reconstruction of the CT volume using direct volume rendering.....	73
Figure 5-2. Examples of CT image windowing and edge enhancement	75
Figure 5-3. Line sampling over an axial CT slice.....	77
Figure 5-4. Surface reconstruction examples of the airway and lungs volumes.....	79
Figure 5-5. Volume reconstruction of CT volumes simulating the beam hardening effect.....	85
Figure 5-6. Reconstruction of chest DRR and internal structure surface	87
Figure 5-7. BEV reconstruction of a patient with neck carcinoma	89
Figure 5-8. OEV reconstruction of a female patient mamma carcinoma.....	90
Figure 5-9. DRR reconstruction simulating megavoltage X-ray energy.....	91
Figure 6-1. Selective combination of RTP volumes	96
Figure 6-2. The geometry of a unit cube	99
Figure 6-3. The geometry of the 64 control points defining the B-Spline in three dimensions ..	102
Figure 6-4. 3D Reconstruction results of phantom data.....	103
Figure 6-5. Simplified diagram of the volume rendering pipeline	104
Figure 6-6. Volume image mixing using single image intensity blending.....	108

Figure 6-7. Target volume and iso-dose volume mixing using the inclusive opacity 109

Figure 6-8. Iso-value representation of the dose volume 109

Figure 6-9. The effect of dose mapping on VOIs surfaces..... 110

Figure 6-10. Illustration of a DVH over four different structures..... 112

Figure 6-11. 3D representation of the DVH 113

Figure 6-12. Merging of CT and Dose volume 116

Chapter 1

Introduction

1.1 Introduction

Cancer belongs to a group of disease characterized by tumor growth and spread, and is the most significant health care problem in European and Western Countries. The clinical processes used to treat cancer can be separated into drug treatments, radiation therapy [Meyer96] (RT) treatment or even a combination of them [Zambo94]. RT uses radiation in order to deliver a very accurate dose of radiation to a well-defined target volume with minimal damage to surrounding healthy tissues. The wanted result is the eradication of the disease and the improvement or prolongation of patient's life. The amount of required dose can be applied on the tumor site using external beam radiotherapy or brachytherapy [Kolot99]. Hence RT is a very demanding process that requires accuracy and affectivity not only for the elimination of the cancer sells but also for the protection of the healthy organs within the human body. In this dissertation it is of interest the radiation therapy process (RTP) using external beam radiotherapy (EBRA).

1.2 The External Beam RT Process

The RTP for malignant disease is complex and can be carried out in several steps. In the following paragraph we will go through these steps and briefly describe each one of them including the clinical specialist and the system involved each time (see Figure 1-1).

1.2.1 Target Volume Determination

The first step on the process is the patient diagnosis. The diagnostic study can be carried out on any diagnostic system including conventional x-rays or a 3D imaging modality like computed tomography (CT), magnetic resonance (MR) or nuclear medicine (Gamma-Camera, PET, SPECT). Follows the very crucial step of definition and localization of the disease (tumour) and its extensions relative to adjacent critical normal organs and tissues (target volume definition). This can be done with several ways, depending on the case study, ranging from simple clinical examinations to complex. In this step the main specialist involved is the physician and the system traditionally used is the treatment planning system (TPS).

For simple cases the X-ray fluoroscopy images produced on the real simulator can be used for the disease localization. For complex treatment cases, the data used are coming mainly from a CT scanner. The CT scanner might belong to the radiotherapy department or to a diagnostic department, but in both cases the CT's table-top must be flat and not curved (which is usually the case for diagnostic CT scanners). Further more, the CT room must be equipped with at least, three laser projectors. This laser arrangement is crucial for the patient alignment and repositioning through the RT process and exists in the simulation and treatment room as well.

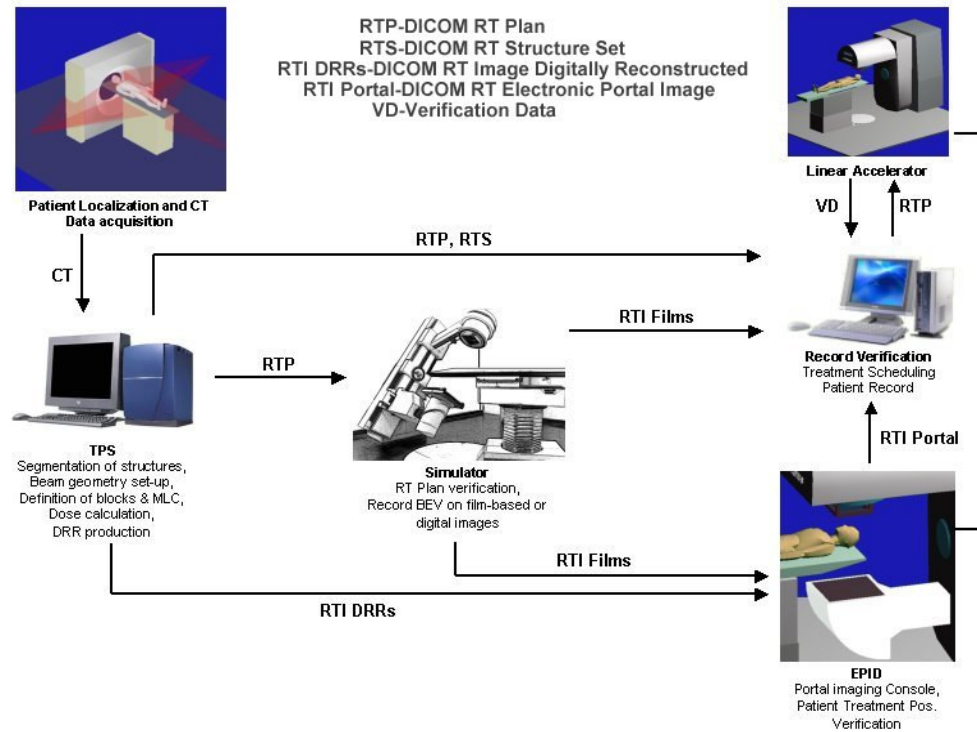


Figure 1-1. RT clinical routine and data workflow for external beam treatment planning and delivery using the conventional simulator.

1.2.2 Treatment Planning

Another step of the process is the radiation field placement, which serves to adequately cover the tumour site minimizing the dose exposure of healthy normal tissues. The specialist involved in this step is the physicist. Having the necessary number of beams placed to the appropriate anatomical location, the dose distribution for this plan will be calculated using the TPS.

1.2.3 Treatment Verification

Treatment verification is the last step before initiating the treatment. At this step treatment plan needs to be confirmed by an imaging procedure to ensure that each beam's location and shape traverses the desired anatomical volume and avoids critical structures as much as possible. The verification process usually takes place on the real simulators or on the treatment machine with the use of the portal-imaging device. In this step two specialists are involved: the physicist and the physician.

1.2.4 Treatment Delivery

The final step of the RT process is the actual treatment delivery, which takes place on the treatment machine (LiNAC) and high-energy photon or electron beams are used. In this step the patient location relative to the laser system is established using the appropriate

table translations and the beam shape and orientation is applied according to the treatment plan.

1.3 Role of Simulation in RT process

The *Simulation* of the RT process belongs to the most important steps of whole treatment process. During Simulation the defined treatment set-up, which is prepared on the TPS, will be simulated on the Simulator using the light field projection and the radiographic or fluoroscopic modes provided by the conventional Simulator. This process will help to mimic the radiation therapy beams in terms of divergence. In principle the Simulation process will optimise the original treatment in order to have the optimum target coverage while minimizing the dose to normal tissues. The final configuration will be recorded permanently on radiographic film.

1.3.1 The Conventional Simulator

Traditionally the device that performs the RT simulation is the Simulator (see Figure 1-2). The Simulator is a machine that emulates the geometry and the movements of the treatment unit but diagnostic quality x-rays instead of high-energy treatment rays. The Simulator has multiple functions and tends to be used somewhat differently in every RT department. The most common functionalities of the Simulator are described with more details in chapter 2. Unfortunately there are a number of disadvantages in the use of the Simulator:

- a) **Image Quality:** Although the Simulator is a useful tool to define the localization of the disease and the surrounding healthy tissues, there are many cases where soft tissues due to their low x-ray absorption are not visible on the fluoroscopy or radiography. To overcome this problem often contrast medium is used. Further more, while using the fluoroscopy mode, the magnetic coils of the Simulator image intensifier suffer from distortions resulting to a distorted final image. Also, the limited size of the image intensifier detector limits the amount of the visualized patient's volume.
- b) **Accuracy:** The Simulator is a hardware device composed of several mechanical parts including the x-rays head, the collimator, the gantry and the treatment couch. The mechanical components often introduce inaccuracies to the Simulation process. Therefore systematic quality control tests are needed. If the component under test does not fulfil the requirements it must be replaced.
- c) **Design Constrains:** The design of the Simulator components is such that they mimic the treatment machine. Even though in some treatment cases it is not possible to perform the simulation because of difference between the LiNAC and the Simulator. One such example is the non-coplanar beam set-up with combined table and gantry rotation. This set-up can be applied on the treatment machine in absence of the



Figure 1-2. Illustration of the conventional Simulator. On the lower right corner the fluoroscopy of the Alderson phantom.

portal imaging component, but not on the real Simulator due to the interference of the tabletop with the image intensifier.

- d) **Clinical Costs:** The installation of a Simulator is a high investment for the clinic in terms of hardware equipment, space, time and personnel. The Simulator must be installed on a room as a stand-alone device. This room of course requires the installation of special components that are necessary for the appropriate function of the Simulator. To manipulate the Simulator at least two specialised persons are needed: a technical assistance and the radiation oncologist. Furthermore the verified result of the Simulator must be recorded on radiographic films, which require an expensive process for their development.

1.3.2 The Virtual Simulator

The alternative to the Simulator device is the use of the Virtual Simulator (VS) or CT-Simulator or 3D-Simulator. Although this concept has been originally introduced, scientifically and clinically, as VS and CT-Simulation in this work we prefer to use the term **3D-Simulation** or 3D-Sim. The reason for that is that the 3D-Sim systems nowadays include several different functionalities that spread much further than the standard volume definition and geometric field planning, which used to be the standard system functionality for the CT-Simulators. In addition one can work using any 3D imaging modalities beyond the CT scanner, such as MR and PET for example.

The simple concept of CT-Simulation was first proposed by Sharehouse [Shero87] and has been characterised as one of the significant technological advances in radiation oncology in the past 20 years. Since today several reports have been written proven the advantage of the 3D-Sim in the RT clinical routine [Nagat90], [Nishi90], [Rosen91], [Perez94], [Perez95], [Vijay95], [Butke96], [Micha96], [Rose96], [Ragan96], [Conw97], [ValiA97], [ValiB97], [DasCh98], [Gripp99], [Vuong00], [Schie00], [McJur01]. More recent studies highlight not only the advantages of the 3D-Sim applications, but further presented results on how well the 3D-Sim packages integrate in the modern clinical RT environment [EdWon02], [Zambo02], [Houst02], [Karan02], [Bolle03], [Dicks03], [Valen03], [VanSo03], [Stras04], [StraV04]. The 3D-Simulation concept is based on the use of the digital patient data, mainly CT slices, instead of the real patient. The patient has to go first through the CT scanner. The laser localizers will be used again here for the definition of the reference point. The projected on the skin laser beams will be marked and aluminium markers will be attached the same locations prior to the CT acquisition. The volumetric CT data then will be imported on the 3D-Sim application and will be used to perform the Simulation process virtually, lack of the physical patient presence.

Similar to the conventional Simulation process, this includes the tumour localisation, placement and delineation of the necessary number of beams and verification of the beam tumour coverage (see Figure 1-3). In chapter 2, we will see that computer graphics science provides the appropriate tools to compose and generate such an environment. The RT process has to be modified and adapted to the use of the 3D-Sim. The main benefits of the 3D-Sim over the conventional Simulator are:

- a) **Absence of the physical patient:** During the conventional Simulation process the physical patient must be present and get positioned on the Simulator couch. In 3D-Sim the patient's electronic data, mainly CT, are used for the simulation. 3D-Sim avoids the often-experienced *bottlenecks* in patient workload flow within a department

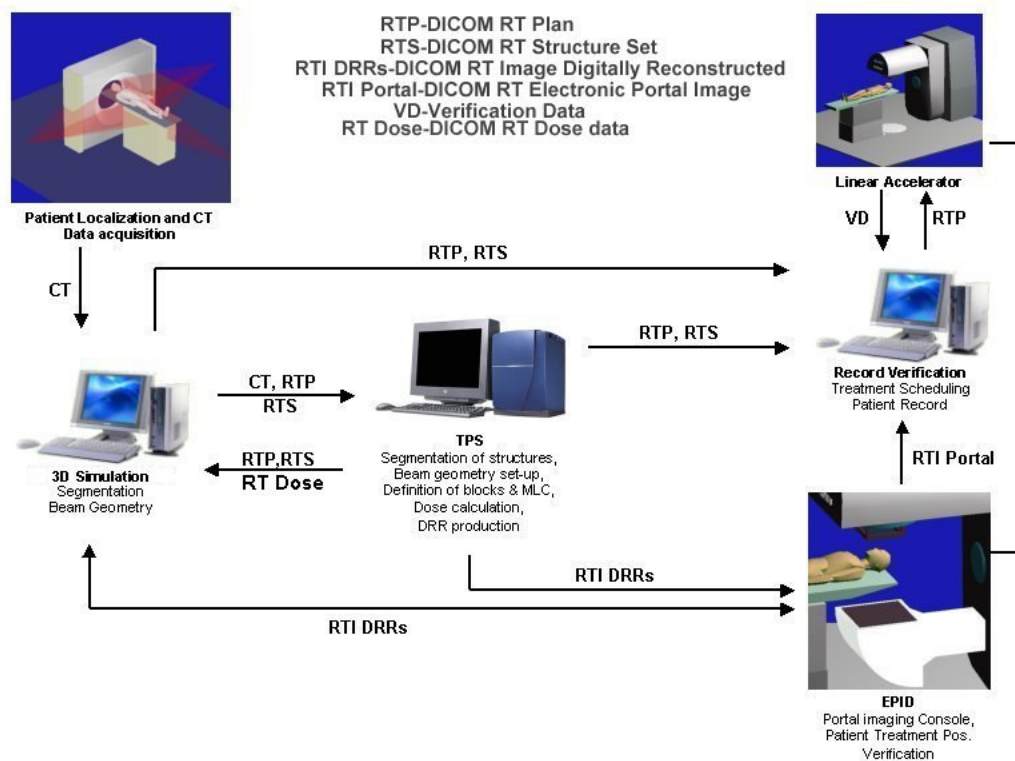


Figure 1-3. RT clinical routine and data workflow for external beam treatment plan and delivery using the *3D-Simulation*. In this clinical environment all information can be transferred digitally lack of X-ray films.

of radiation oncology and reduces the systematic error caused due to the patient's re-positioning on the Simulator's couch.

- b) **Reduced Simulation Time and Personnel:** Using the Simulator the average time needed to perform the Simulation process is about 20min. The 3D-Sim provides tools and technique that can reduce the time needed for the Simulation process up to 50%. In addition the only professional involved to the simulation process in the radiation oncologist.
- c) **Less Constrains:** 3D-Sim will never face the problem mentioned in paragraph (1.2.1-c). The component limitation of different treatment units can be adapted by the 3D-Simulator and additionally collision detection algorithms can be applied as well in order to verify the geometric treatment validity.
- d) **Advanced Visualization:** As already mentioned the Simulator can verify the simulation process using the light field projection and the 2D radiographic image. The 3D-Simulator can reconstruct the computerized reconstructed radiograph (CRR) in real time and simulate this way the fluoroscopy mode of the Simulator. CRR has a number of benefits against the conventional fluoroscopy, like the large field of view that can be used to reconstruct the patient volume and the selection of the tissues that will contribute to the reconstruction of the final image. In addition 3D-Simulators can visualise as super imposed structures on the CRR, the target volume and the or-

gans at risk. The multi planar reconstruction views provide an ideal navigation tool to investigate complex anatomy within the patient's volume.

- e) **Lower Investment:** Finally the 3D-Simulator is a lower investment for an oncology clinic in terms of money and space compared to the real Simulator. The only hardware needed is a personal computer (PC). The final treatment set-up can be recorded digitally or as hard copy on conventional printing paper.

1.4 Related Work

Although the idea of 3D-Sim is relatively old, only the last few years these systems became popular. The main reasons for this wave are the advances in CT technology and computer hardware technology. The invention of spiral CT was a great step towards high-speed acquisition of CT data. These days the reconstruction time of a slice for a conventional CT scanner can reach the times from 0.75 to 0.45 sec. Hence the acquisition of high-resolution volume data can be done within a few hundred seconds. Most oncology clinics will potentially obtain their own CT scanner since the CT imaging modality has become the standard modality for the oncology clinics nowadays.

The advances of the low cost computer hardware technology on the other hand, mainly processing power, graphics libraries supported by hardware and memory, allow the processing of larger volumetric data within real time. Last decade, when 3D-Sim systems start to be presented, it has been reported [Shero90] [Shero91] that the DRR images were calculated only after the definition of the final beam configuration, due to the high computational cost. A few years later different authors [Culli93] presented a near to real time calculated DRR. They used reduced interpolation rate for the ray casting applying nearest neighbour sampling. For a volume data with resolution $V = (X, Y, Z) = (256 \times 256 \times 128)$, the preview image needed about 1sec to be reconstructed and the final high quality $I_m = (U, V) = (512 \times 512)$ pixel image was completed after 5-6sec. Galvin in his study [Galvi95], used a volume data set of $(X, Y, Z) = (512 \times 512 \times 50)$, and manage to compute a $(U, V) = (512 \times 512)$ DRR image in 8sec. The hardware platform used for the experiments was a Voxel Q with the processing power of 10 million trilinear interpolations per second. A standard CT data acquisition performed on a spiral CT, contains typically 80-100 slices equally spaced to 3mm each, with grid resolution (512×512) . Currently to reconstruct this amount of data on a 1GHz processor requires less than 4 secs. High-resolution CT data offer the possibility to render high quality DRR images, approaching the spatial resolution of the real X-ray images produced by the conventional Simulator. Further more high quality data sets allow the visualization of any complicate anatomy in surface or transparent modes. Advances in both technologies, CT scanner and processors, promote the use of the 3D-Sim. We have to clarify that some 3D treatment planning systems offer 3D-Sim functionality with limited capabilities. The reasons that are:

- a) The complicate design of the systems that require a well trained user to perform the simulation and planning and
- b) The limited visualization capabilities they offer in comparison to 3D-Sim systems.

These systems are designed for physicist, scientists who are educated in use of software and computers. In general TPS systems are complicated due to their purpose, which is the dose calculation. This is the main reason why TPS systems are rarely used from physicians. Dose calculation algorithms on the other hand require high processing power in relation with the amount of data used: the less data used the faster the calcula-

tions will be completed. Thus even nowadays TPS systems can handle limited amount of data. It is common understanding that limited data resolution result to limited anatomical information. In addition for the dose calculation algorithms a surface representation of the organs of interest is required. These organs involve the body contour, the target volume and the organs at risk. Therefore these systems use basically polygon-based techniques to represent anatomical structures in 3D.

Currently there are a very small number of the dedicated Virtual Simulator (VS) systems, such as AcQsim [AcqSim], AdvantageSim [GE], [Schie00], SmartSim [SmartS], FocalSim [FocalS]. A direct comparison of between these systems it is relatively difficult to be performed. The major weaknesses or deficiencies of the current 3D-Simulator systems are:

- a) Complicated user interface and therefore reduced effectiveness in user-software interaction.
- b) The lack of auxiliary tools for volume definition as well as for the realization of the simulation plan.
- c) In some cases limited visualization capabilities is also an issue that reduces the system performance.

User interface is a critical issue for every software system. 3D-Sim systems are complicate software with dedicated functionality. If such a system is designed with complicated user interface, the result will be the requirement of extensively training for the users as well as the complicated and time-consuming interaction. Further more the lack of effective and interactive volume definition and beam editing tools will increase the time required to simulate a treatment plan. Limited visualization capabilities might affect the outcome of the patient treatment since the high-resolution data will be less comprehensively examined from the physicians in order to localize accurately all areas of interest.

1.5 Challenges in 3D-Simulation

Although the idea of the 3D-Sim is relatively old starting from the early eighties there is still areas for improvements. Advances in technologies of radiation oncology and diagnostic imaging modalities demand the adaptation and the refinement of the 3D-Sim systems to the new technologies. In the following we will focus only on some of the challenges in the 3D-Sim and radiotherapy treatment planning, that this thesis contributes.

- **General considerations:** A very important issue is the demand for compatibility, flexibility, interactivity and user friendliness of the 3D-Sim system. The appropriate system design and the platform selection are critical in order to guarantee system compatibility and flexibility. The 3D-Sim systems must be designed for users who are not computer experts. In addition a 3D-Sim system must be capable to import large amounts of data, to process them in real time and easily manipulate them. In addition the synergy of several functional tools is critical to assure the best clinical outcome. For example the accurate visualization of the irradiation field guaranties accuracy during plan verification. Therefore the field must be reconstructed in two and also in three dimensions together with the patient volume data. The most important issue here is the visualization of irradiation field as a light projection on the patients skin. This is the most common way for verification of the field location on the external patient anatomy.

- **Interactive Volume Segmentation:** The interactive definition and visualisation of volume of interest is a demand for every 3D-Sim and treatment planning system. A special condition exists in 3D-Sim since high-resolution digital data are used. This is of great benefit for the physicians especially in cases where they have to investigate complex anatomy. But when it comes to the definition of the target volume and the organs at risk the process becomes laborious since traditionally this process takes place on the 2D axial anatomic plane stepping slice-by-slice. In addition the segmented volumes must be visualised accurately and fast.
- **Motion Artifacts Correction:** The greatest challenge probably in cancer treatment and visualization techniques is the compensation of the motion artifacts and the prediction of the moving organs during data acquisition. Although the reconstruction time for the CT scanners has been tremendously decreased, there are internal organs that their movement might cause rigorous blurring artefacts on the acquired CT images, since their deformation speed is higher than the acquisition speed. In addition the CT scanner acquires the digital images of the patient at a time moment. This means that although the internal organs are moving we see their location in space just at one moment in time. In this work we will concentrate on the reduction of the breathing artifacts that cause deformation of the skin surface.
- **Imaging:** The main difference between 3D-Sim and TPS systems is that the later perform the dose calculation and the plan optimisation according to the dose distribution on the target volume and the organs at risk. For that reason the role of 3D-Sim is getting confused, although VS provides superior quality on visualization aspects. Therefore there is a great challenge on finding techniques that can provide optimum qualitative evaluation of field configuration based on the geometric parameters and also on the dose distribution in relation to the treatment organs.

1.6 Summary and Contributions

This dissertation results from the research work while designing and implementing the 3D-Sim system called *Exomio*. Main attention is given to techniques, which increase interactivity, accuracy and liability of the 3D-Sim system, in order to provide solutions to most of the problems addressed as challenges in the previous paragraphs.

The next chapter, Chapter 2, gives a brief overview of state-of-the-art in the 3D-Sim systems. In addition the concept of the 3D-Sim in the clinical routine is presented, as it has been established in most of the oncology clinics these days. Further more the appropriate components needed to construct a 3D-Sim system are presented. These tools involve the hardware and software platforms, the user interface and the graphic algorithms needed for the realization of the 3D-Sim. For example different transfer functions that can be used for the reconstruction of the DRR images are analysed as well their advantages and disadvantages against the real X-ray images.

A number of volume definition issues are presented in Chapter 3. As previously mentioned volume definition is the most important step of the treatment planning process. The reason of course is that for the most treatment cases, the shape and location of the target volume is a crucial factor for the irradiation field configuration. Chapter 3 presents the most common techniques used for defining structures in radiation therapy. A novel technique for volume definition is introduced, that uses closed planar contours from orthogo-

nal planes and gives the ability to generate 3D anatomical shapes with minimum user effort when compared to the traditional 2D slice-by-slice procedures. In addition a semi-automatic algorithm based on 3D contour tracing that can detect the spinal cord anatomy is presented and evaluated.

Chapter 4 describes a novel approach on compensating the surface respiratory artifacts produced during the CT acquisition. Briefly the patient's surface is used in several calculations in radiation therapy, mainly for treatment verification of the patient positioning. The value daily measured in clinical practice is called source-to-skin-distance (SSD) and represents the distance between the irradiation source and the patient skin along the iso-center axis, for the current field configuration. The calculated SSD values under standard conditions are affected from the respiratory process of the patient, which is recorded on the acquired CT data. Our algorithm will cause a shape refinement of the cross section contours that are used to define the body surface.

Volumetric visualisation has been always a challenge in radiation therapy and especially in 3D-Sim. Chapter 5 presents visualisation techniques that assist the RT process. We focus mainly on the 3D reconstruction of the thoracic region using CT data, which is especially interesting since it contains structures with very different tissue densities. A new interactive method is presented that isolates the lung volume in the pre-processing step of the volume visualisation pipeline. In addition multi-volume visualisation techniques are presented in order to visualise simultaneously the CT data volume, the target volume and the treatment field geometry, enhancing on the maximum information an observer could retrieve using volume rendering techniques.

In Chapter 6 we will present the visualization workflow that describes an integrated 3D irradiation dose display process within the 3D-Sim environments. The work of Chapter 6 is separated in two main parts: the dose re-sampling and dose visualization part. The first part involves the interpolation of the original dose volume data; a critical step when aiming to produce accurate calculation results as well as high quality 3D illustrations. The second part involves the mixed visualization between the dose and the CT-volume in two and three dimensions. Volume rendering is the vital component used for the implementation of the visualizations tools that will be presented, and aim to augment the qualitative verification of the dose distribution, the volumes of interest and the CT data.

The conclusions of this work can be found in Chapter 7. The research work of this thesis rose as challenges from the design and implementation process of the 3D-Sim called *Exomio* [Exomio], [Karan01], [Zambo02]. Some of the challenges in 3D-Sim have been addressed in this work and the results represent state-of-the-art components for a 3D-Simulation system. Nevertheless there is always place for improvements and future research.

Chapter 2

3D Virtual Simulation: System Concept

2.1 Introduction

The RT process is demanding and complex, composed of several steps that have been already described generally in chapter 1. One important step in this process is labelled as *simulation*. Repeating the principle of simulation, it is basically the localisation of the target volume, the area that will receive the maximum amount of dose, and the organ at risk, volumes that must receive the minimum dose. Once these structures have been well defined, the next step is the definition of the irradiation fields in relation with the target volume and the organs at risk. In addition during treatment the patients receive their therapy via a number of fractions. Therefore there must be a confirmation that the irradiation orientation and the structure localization have remained unmodified.

Both steps described above can be performed on the conventional simulator. There are studies shown that the use of the sophisticate treatment techniques including the use of the treatment simulator, improve the patient outcomes in contrast to treatments that lack the simulator. In other words it has become the last two decades a common understanding that the simulator is an essential component in the RT. The last decade there is an evolution in the technology of the computed tomography scanners (CT) that tend to become more common in the radiotherapy departments as part of the standard equipment. Part of this evolution is also the use of the 3D-Sim software systems that together with the CT scanners and some additional equipment integrate the clinical procedure called CT-Simulation. Nowadays the 3D-Sim systems fulfil or even go beyond the criteria of a real simulator for most treatment cases, replacing in many radiation oncology departments the later.

The information and functional level of a 3D-Sim software, should be comparable with that of a real simulator and further more it should provide high quality imaging algorithms for 3D data visualization and manipulation. In addition they aim to “virtualise” the real clinical environments of the RT process up to a level. This means that there are several procedures that must be simulated and modelled and these can be separated in two groups:

- a) Simulation of the mechanical movements of the real machine. This includes the rotation of the components gantry, collimator and couch, as well as translation of the couch table-top to the directions vertical, lateral and longitudinal. The manipulation of these components is necessary in order to achieve the optimum field configuration for each treatment case.

- b) Reconstruction of the same type of images produced from the conventional simulator and LiNAC machines¹ (the differences of the two systems LiNAC and Simulator have been given in chapter 1). This involves the generation of digital reconstructed radiographs, simulating kilovoltage and megavoltage X-ray images. The generation of a real 2D X-ray image, is based on the attenuation of the energy of the X-ray beams while they are travelling through a material, and in our case through the patient body. The attenuated beam energy is detected on the X-rays radiographic film or on the surface of the image detector or intensifier. Since several decades these 2D X-ray images are used for localization and treatment verification in radiation oncology.
- c) Reconstruction of the patient's surface, external or internal anatomy, using the digital patient data sets, coming mainly from the CT scanner. This concept is important due to the lack of the physical patient. These images can be used for verification purposes in order to detect the interaction of the treatment beams with the patient's body.
- d) Modelling of the irradiation machine or the simulator machine including patient orientation. This information will provide an overview of the simulation process, indicating in approximation the localization area of the patient for the specific treatment as well as the orientation of the patient on the treatment couch.

This chapter is separated in two parts. In the first part the hardware components of the real simulator and their role is briefly described so as to better clarify the functionality of the real machine. In the second part the minimum required tools that can compose a virtual simulator system are described.

2.2 The Treatment Simulator

The treatment simulator serves two purposes in the oncology department: as tumour localization tool and as a verification tool adapting the same treatment configuration and patient localisation, as would happen on the treatment machine. An industrial simulator (Elekta) for external beam radiotherapy is illustrated in Figure 2-1. Nowadays several industrial vendors provide real Simulators, with special mechanical features in order the simulator to be adapted to different LiNAC configurations. For many years the film-based simulation (digital images are acquired through digitisation of radiographic films), was adequate and thus there have been very few improvements in the technology of the treatment simulators. However in recent years the need for digital simulation image has grown significantly following the new innovations in radiotherapy technology such as computerized multileaf collimator, electronic portal imaging device, and networking of patient data. The direct acquisition of digital images during patient simulation, allow an immediate, easy and efficient association of the above-mentioned information in combination to the treatment simulation information [Atari95].

The most advanced development of the simulator involves the conversion/upgrade of the treatment simulator to emulate digital volume acquisition as done using the cone-beam CT. Cone-beam CT performs direct 3D reconstruction from a set of 2D projection data obtained with a cone-shaped beam geometry, in contrast to the conventional CT where 1D projections are obtained with a fan-beam geometry and are used to reconstruct

¹ Since the two systems, LiNAC and Simulator have the same geometry, any movement performed in one machine coincides absolutely on the other. There for we have to simulate only one of them. Their main difference is at the energies they are using and therefore at the X-ray images produced.

2D information [Smith90]. The cone-beam volume reconstruction in radiotherapy has been proposed from several authors. The idea has been applied on the simulator [Cho98], [Verel99], [Agost01] as well on the treatment accelerator. In the first group, which is of our concern, the aim has been the integration of the Sim-CT functionality in the clinical routine attempting to replace the digital data acquisition using the conventional CT scanner. A typical diagram of the hardware configuration of the radiotherapy simulator as proposed in [Cho98] is shown Figure 2-2. Important components in this configuration are considered the digital fluoroscopy unit (digital spot imager or DSI), commonly used in diagnostic imaging and the volume CT reconstruction algorithm combined with the distortion correction algorithm. To improve image quality, the digital simulator images have been acquired using pulsed X-rays at high tube current. Unavoidable geometric distortion influences the image appearance due to the imperfection of the electron optics and thus was necessary to correct for geometric distortion before applying the CT reconstruction algorithm.



Figure 2-1. An industrial simulator type from Elekta.

An additional problem is also produced from the limited size of the detector, which restricts the application to be used in large body sections. Verellin *et al.* in their work [Verel99] used a detector array composed of 288 cadmium tungstate single crystal scintillators attached externally to the simulator image intensifier. That configuration was free from distortions and in addition one could select three different kinds of fields of view (25cm, 35cm and 50cm). The results of their work showed that the HU values produced in the volumes generated using the cone-beam simulator are very near to those produced from the CT scanners and thus dose distribution can be also calculated with good precision. The integration of Sim-CT in the clinical environment was successful up to a level. The limitations are coming mostly from the mechanical components such as the high current required for the X-ray tube, the limited field of view on the acquired volumes was a result of the detector size. In addition the data processing and the volume reconstruction phase is really time consuming for high-resolution volumes.

The image detectors and the X-ray technology continuously improves and probably some of the above limitation will be solved within the next few years. In any case the product of a Sim-CT is a reconstructed high-resolution volume that will be used to feed a TPS or a 3D-Sim software. It is common that the 3D-Sims are preferred due to their ability to deal with large amount of data. The clinical workflow where the Sim-CT is used is still a research topic and only in a few centres. Usually in the standard clinical routine an average of four to seven digital images are acquired during treatment simulation. The 3D-Sim can be used as a replacement or add on to the conventional radiotherapy simulator. In either way it is for sure that 3D-Sim can improve the treatment planning workflow. In the next paragraphs we will go through the most important mechanical parts that com-

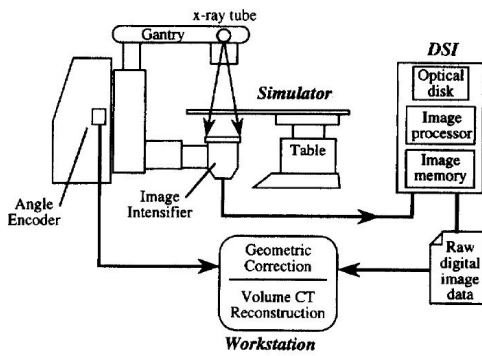


Figure 2-2. Hardware configuration of the digital radiotherapy simulator.

the patient), which are penetrated by X-ray. Using the LiNAC, these structures will be irradiated by the radiation source, if the LiNAC is set by the same parameters as in the simulator. This is a very important tool for physicians to investigate the relationship between beam and patient tissues (including tumor, and other critical organs). Besides this image, physicians also can use their views to check the motion of the machine and the radiation projection area on the patient body. The former is what the detector sees, which is called Beam's Eye View (BEV), and the later is what physician sees, which is called Observer's Eye View (OEV). Both BEV and OEV are basic visual information in RTP.

2.2.1 Simulator's Gantry

The gantry is a common part for the simulator and the LiNAC, with similar geometry and the same degree of freedom. Nevertheless internal and external components are very different for both systems. In a simulator the gantry hosts the low energy diagnostic X-ray source, the collimator, the light source, the wires for the generation of the treatment field, the block tray and the image intensifier. In contrast the gantry of the LiNAC hosts, the treatment source, the collimator that defines the shape of the irradiation field, the multi-leaf collimator (MLC) if available, the block tray and the portal imaging device.

In the real simulator the X-ray source is responsible for the generation of the appropriate energy of photon beam. The shape of the irradiation beam can be modified using the collimator, the lead blocks or the MLC. The direction of the irradiation field can be changed by rotating the gantry or the collimator. The gantry can perform rotations around the axis Yf as can be seen in Figure 2-3 and the collimator around the Z-axis.

As already mentioned, the "head" of the simulator's gantry host a normal light source that is used for verification purposes and as an indicator of the irradiation field. The light field is always activated prior to the generation of the X-ray image, indicating the field shape and orientation projected on the patient's skin. The light field verification is the most important visual tool used for the verification of the field orientation and shape relative to the patient position.

pose the simulator. We will describe their geometry and function in order to better understand which functionalities must/can be simulated from a software system and how.

In the hardware configuration diagram of Figure 2-2 one can notice the main mechanical simulator components, which are: the simulator's gantry (hosts the imaging components) and the simulator's couch (composed by the table top and the table support). When patient lies down on the simulator's top table, X-rays are emitted from the irradiation source of the simulator, passing through the patient, and detected by image receptor. The detected X-ray image presents the structures (parts of

2.2.1.1 Imaging Components

In this paragraph we will try to briefly describe the components that contribute to the generation of the X-ray image on a treatment simulator. To perform a comparison of the virtual generated X-ray images, DRR and MIP, with the real X-ray images produced from the simulator we have to focus to those components that affect the image quality. To generate X-ray images on the real simulator the same principle and components are used as in diagnostic imaging. The major components involved are: the high voltage generator, the X-ray tube, the image detector (or image intensifier), the video display monitor, the film cassette and the X-ray film. The real simulator allows the generation of two types of X-ray images: radiographic (static) images that are captured on the X-ray film and the dynamic real time fluoroscopy, that allows the observation of internal organs and structures in relation to time.

However, if we compare the diagnostic imaging and the radiotherapy imaging, there is a major difference between the two techniques. That is the large distance between the focal spot and the image intensifier for the simulator. This distance varies on the simulator between 100cm to 170cm depending on the treatment case, and results to attenuation of the beam intensity at a high level, increasing scatter to the detector. Although techniques have been developed to compensate the scatter effect it still remains a major reason for generating low quality X-ray images.

The image detector can be also a reason for mechanical collisions, which are another constrain of the real simulation especially in cases where the couch and gantry are rotated. Figure 2-4 illustrates such a case. The collision is coming from the image intensifier, which is located on the lower end of the simulator's gantry. Although this treatment case can be applied in the treatment machine, the real simulator cannot handle it.

As previously mentioned the real simulator can generate real time X-ray images (fluoroscopy mode) and static. Although real time images have a great advantage against static there is a limitation in the design of the X-ray generators, since fluoroscopy mode takes much more time than radiographic exposures. In order to avoid melting of the generator a much lower tube current must be used. Further more for wider heat spreading on the target a double focal spot is used, larger in the case of fluoroscopy than the radiographic exposure. The impact of the larger focal spot is that objects will appear to have "blurred" edges due to larger penumbra.

The component that cooperates with the X-ray beam to generate the real time images is the image intensifier. The use of the image intensifier gives the ability while the fluoroscopy mode is on to move other com-

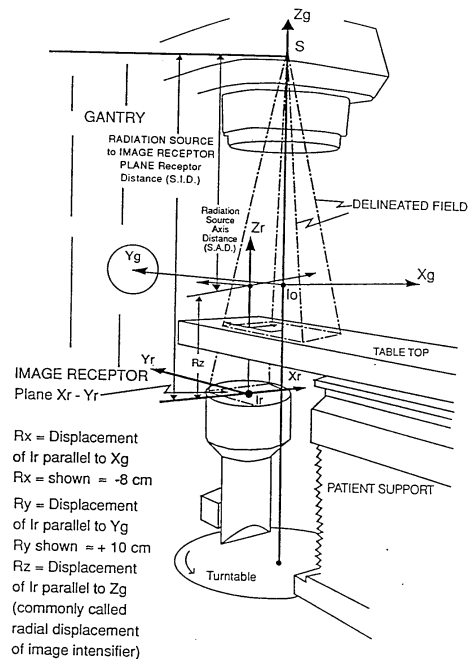


Figure 2-3. Basic simulator components and coordinate system as defined from IEC 1217

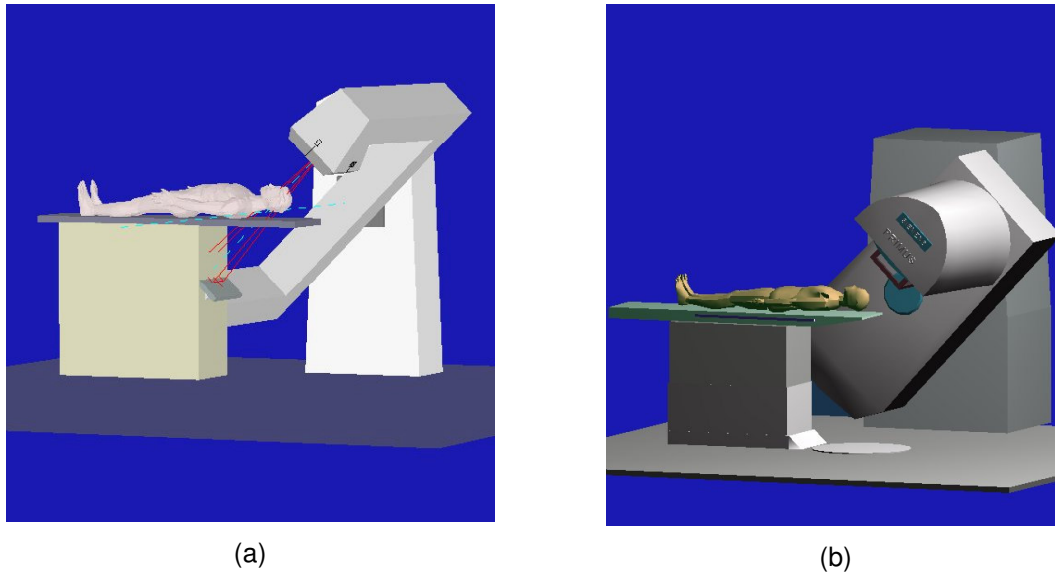


Figure 2-4. Simulated collision for a simulator model based on IEC 1217 (a) and a Siemens LINAC model (b). The table is rotated isocentric 90° and the gantry 45°. On the conventional simulator this case cannot be simulated since the image detector would collide with the table support (a). However on the treatment machine this case can be applied (b).

ponents of the simulator, like treatment couch, gantry, collimator and so on, and to investigate optimum localization positions for the current treatment case. Analyzing the structure of an image intensifier is beyond the scope of this work. Here we will try to see the limitation of the image produced from the image intensifiers in contrast to the virtually reconstructed X-ray images. Indeed the greatest constraint of the image intensifier against the use of 3D-Sim, which uses data coming from CT or MR scanners, is the limited field of view that offers. This restriction results from the mechanical components that compose the image intensifier. The diameter of the field of view ranges between the 23 and 40 cm. Furthermore the X-ray images produced for the image intensifier suffer from geometrical distortions, due to lens optics or electron optics (see Figure 2-5).

Finally the image quality is highly influenced by the veiling glare. Briefly the veiling glare creates a uniform over the entire field of view of the image intensifier. This effect is enhanced in cases where minimally attenuated and highly attenuated structures are exposed simultaneously on the field of view. To compensate this artifact usually they close the jaws of the collimator, when this is allowed from the treatment case, creating an even smaller field of view.

2.2.2 Simulator's Treatment Couch and Couch Table Top

The treatment couch is separated into two parts the couch support and the couch tabletop. The couch (or table) support is responsible for the vertical movement and the eccentric rotation of the table. The tabletop is responsible for the lateral and longitudinal translations and also the non-eccentric table rotation. The simulator's table is different from the LINAC table in several senses. Material is an issue of less importance. What mostly counts are other metal parts that compose the table top and are used for the mechanical stability and strength. Assuming now that a treatment field is planned using a treatment

planning system, then applied on the simulator for verification is approved. However if during patient set-up on the LINAC a metallic part of the table-top interferes in the field prior to the patient then the plan cannot be applied.

2.3 3D-Simulator: System Concept

The 3D-Simulator of RT process has a different concept and different functionality compared to the real simulation. The 3D-Sim is fully performed using a system-software and thus digital information are used instead of the physical patient its self. The primary data can be collected from a CT device means of axial slices that compose a volumetric grid with a specific resolution depending on the treatment case. For the processing, manipulation and simulation of real incidents in radiotherapy, 3D visualization technique must be employed. Stand-alone 3D visualization techniques are commonly used in medicine to generate images that will be used in diagnosis or treatment [Sakas01]. Most common application involve the 3D volume visualization stations where the medical data are used

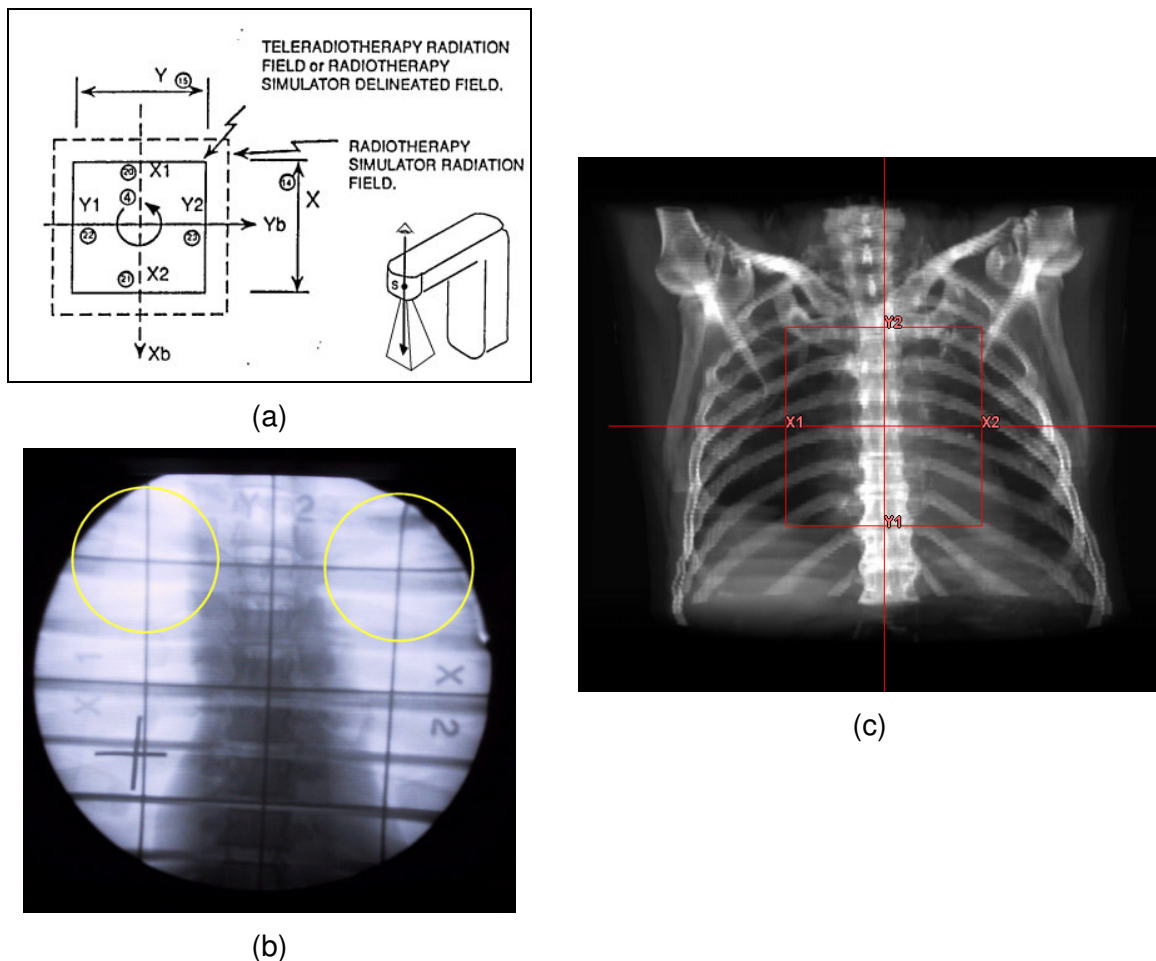


Figure 2-5. Definition of the real Simulator treatment field. In (a) a sketch of the treatment field as viewed from radiation source down to the radiation field. The image in (b) is captured from the image intensifier of the simulator using a wooden phantom as subject. The yellow circles indicate the deformed edges of the field. In (c) an illustration of a DRR with overlay of the treatment field, lack of distortions.

coming from different imaging modalities, and reconstruct 3D images for diagnosis on lesions. In order to generate a system for dedicated medical purpose a more complicated design and combination of state-of-the-art visualization tools is required. Computer graphics science, offers great tools that can be further developed and composed in order to finally create a system. As in several medical imaging applications, the implementation of a 3D-Sim requires the use of simple 2D procedures like line drawing, polygon scan conversion and pixel tracking up to 3D volume rendering and polygon modelling techniques. An overview of a 3D-Sim is given in Figure 2-6. The system is composed of two main parts; the system database and the functional 3D-Simulator. The database is responsible for performing DICOM data communication and storage. That includes normal DICOM imaging data and DICOM radiotherapy structures such as treatment plan parameters, segmented structures and treatment dose volumes. This information is communicated from and to the 3D-Sim system. The functional part of the 3D-Sim involves the memory storage of the digital information and of course the generation of all necessary new structures involved in the 3D-Sim process. Responsible for the generation of this information is considered the user who can manipulate and modify most of them. During data manipulation or interaction the system is responsible for the 2D and 3D display of the treatment information. Finally the system can export the produced information in digital or hardcopy format. The next paragraphs provide an overview of the visualization components that should be considered as essential for a 3D-Sim system.

2.3.1 Volume Rendering: An essential part in 3D-Sim systems

Volume rendering is the technique according to which a scalar field of data with discrete values, volume data, is selectively sampled in order to generation a useful image in relation to the sampled values. A volume data set is typically a set of discrete samples of one or more physical properties in a limited object space, $V(x)$, $x \in \mathbf{R}^n$, in which $\{x\}$ is a set of sampling points; n is the dimension of the sampling space, usually $n=3$, i.e. 3D volume data; V represents the sampling values, it can be a single-valued or multi-valued function. According to the distribution of sampling points (i.e. the structure of x), volume data sets are classified into structured and unstructured data sets. In medical imaging, volume data is usually a structured data set, typically organised as a stack of slices; V can be single-valued (e.g. the CT Hounsfield value) or multi-valued (e.g. density, T_1 , T_2 in MRI). The resulting data structure is an orthogonal 3D array of voxels, each representing a sampling value.

A general pipeline of volume visualisation in medicine can include several steps [Sakas93]. Depending upon the application field, individual-processing steps may be neglected, combined, or reversed. Important to notice is that the final 3D rendering image can be obtained in two ways: either through the intermediate surface representation or through the volume representation (i.e. direct volume rendering). In general, pipelines employing the intermediate surface representation are collectively called surface-based visualisation techniques, as opposed to voxel-based. In addition the reconstruction modes can be separated into parallel, the Observer Eye View (OEV) and the perspective projection, Beam Eye View (BEV). The importance of these visualization tools have been addressed from several studies in different periods [Nagat90], [Purdy93], [Kalet97], [Gerst99], [Grees00], [Schie00], [Killo01], [McJur01], [Houst02], [Zambo02], [Dicks03].

2.3.1.1 Transparent modes

Two are the most common transparent modes used in medical visualisation. The Digitally Reconstructed Radiograph (DRR) and the Maximum Intensity Projection (MIP). In this paragraph both rendering methods will be briefly described, but focusing mostly on the virtual X-ray reconstruction since this is the most important image for the physicians that have been trained for years to use this kind of images for orientation and planning.

Maximum Intensity Projection (MIP): MIP is used in angiography, CT based or MR based. Nevertheless can be also applied to conventional CT, MRA and also to 3D-ultrasonic data sets. Using MIP one can reconstruct images emphasising to structures with high density within the data set. The difference between MIP and other volume shading models is that, in MIP only comparison between voxel values is requested, accumulation and opacity blending are not employed (we call other models as accumulation models). Due to the difference between maximum comparison and accumulation, most MIP algorithms use only ray casting to traverse volume data and select the maximum value among all accessed voxels along a ray. Using ray-casting techniques, one has to traverse

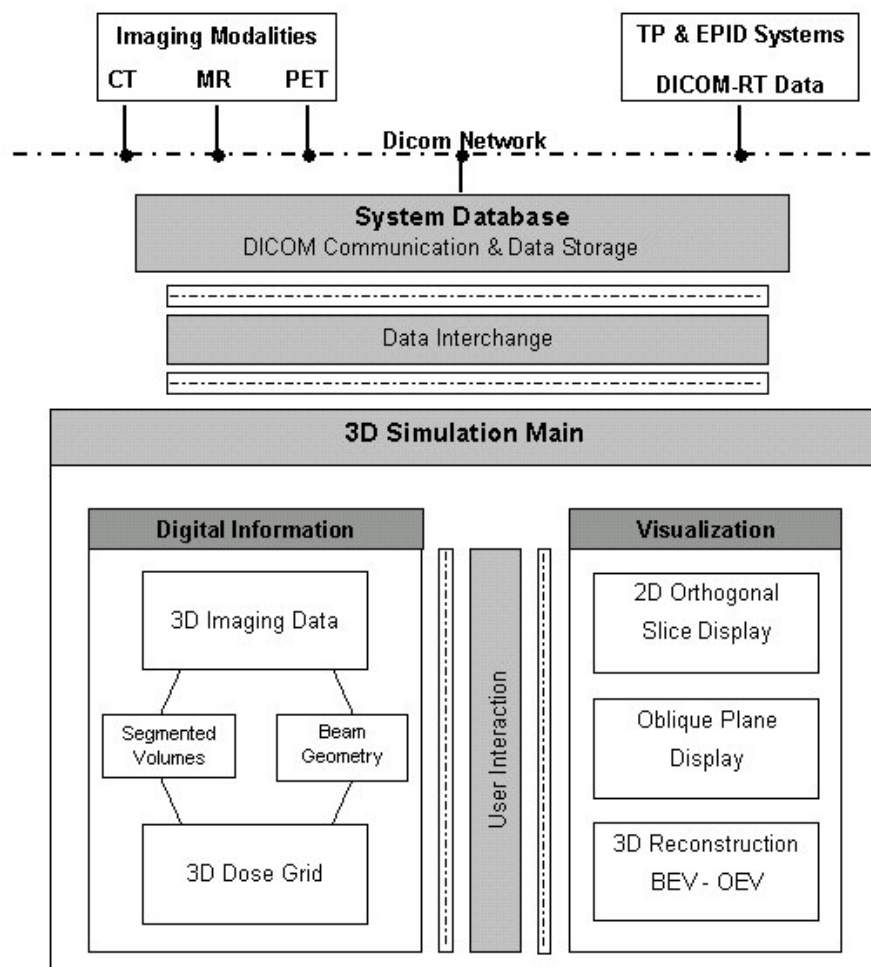


Figure 2-6. Simple block diagram of the 3D-Simulation system for radiation therapy.

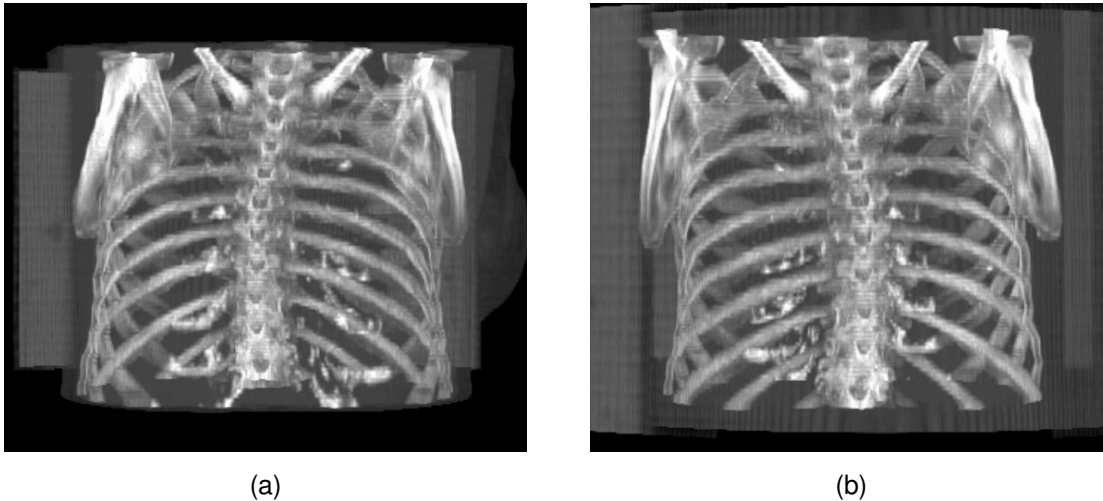


Figure 2-7. Reconstruction of a CT chest volume using MIP. In (a) MIP reconstruction of the chest is presented using perspective projection with gantry angle 0° . In (b) the same principle and data are used but gantry angle is set to 180° . Bony structures are enhanced but depth information is missing.

all voxels on a ray in order to select the maximum value among them. Using MIP, structures with higher data value lying behind an object with lower data value will appear in front of it. The most common way to assist the interpretation of such images is to animate them or interactively change the viewpoint while viewing the data set. An example of MIP reconstruction is illustrated in Figure 2-7. The CT volume is reconstructed from two different viewing directions: 0° and 180° . In both cases bony structures are enhanced but depth information is not preserved. The scapula bones are displayed as they are in the front of the chest bones. In reality this is the case only when the chest volume is viewed from 180° .

Several researchers contributed to optimise MIP reconstruction. Sakas *et al* [Sakas95] evaluated cell maxima only if the maximum value of the examined cell is larger than the ray-maximum calculated so far. For additional speedup they use integer arithmetic for ray traversal and a cache-coherent volume storage scheme. Zuiderveld *et al* [Zuide95] used a similar approach in order to avoid trilinear interpolations. Cells containing only background noise (usually rather low values) are not interpolated. For further speedup a low-resolution image containing lower-bound estimations of the maximum of pixel clusters is generated before the main rendering step. Heidrich *et al.* used conventional polygon rendering hardware to simulate MIP.

Other approaches exploit the advantages of shear-warp rendering 5 to speed up MIP. Cai *et al.* [Cai98] incorporated an intermediate “worksheet” for composing interpolated intensity contributions of voxels for projection of a single slice of the volume. The worksheet is then combined with the shear image to obtain the maxima. However the shear warp rendering approaches do not allow the reconstruction of perspective projection. Morz *et al.*, [MorzH00] showed that many of the voxels do not contribute to the MIP image. By identifying them prior to reconstruction significant speed is gained. Further more Morz *et al.* [MorzK00] presented a method for generating high-quality MIP images (parallel projection), using trilinear interpolation within cells. Their method was much faster than conven-

tional brute-force MIP reconstructions and comparable optimized techniques. This speed-up is accomplished by using an alternative storage scheme for volume cells (sorted by value) and by removing cells, which do not contribute to any MIP projection (regardless of the viewing direction) in a preprocessing step.

Digitally Reconstructed Radiograph (DRR): On the conventional simulator during fluoroscopy mode only a small part of the patient's anatomy can be visualised. This drawback comes due to the limited size of the detection surface of the image intensifier. On the radiographic film this problem is improved but those images suffer from other limitations. 3D-Sim offers unique features that no conventional X-ray system can provide. This comes basically due to the use of CT data, where the patient anatomy is captured using different field-of-view specifically selected for each study. The reconstruction of whole patient anatomy is of great benefit for the physicians.

DRR images are also important for comparison and verification purposes with the portal-imaging device of the treatment machine [Mock99]. The portal imaging device is used as the last step before the irradiation procedure for verification and localization of the patient position. To produce an image on the portal imaging device high energy X-rays are used. The quality of these images is relatively poor since the tissue discrimination at high energies is very low. 3D-Simulators must produce the same type of images in order to be able to compare their simulation result with the treatment position.

DRR images generated from CT digital volumes are often called using the term digitally reconstructed radiographs (DRRs). The term DRR is used when we refer to those X-ray images that are generated with an unrealistic way using direct volume rendering techniques or to those images that are generated from volume data using a better approximation of the physical model. In both cases we try to simulate the attenuation of the X-ray through a medium, in our case through the digital patient's body. This can be achieved by using different transfer functions simulating the classical way of X-ray image reconstruction.

Assuming that a ray with initial energy I_0 enters a volume, which has a thickness of Δs , and is composed from different materials (see Figure 2-9). Using discrete values the final energy of the ray is a product of the following equation:

$$I(s) = I_0 \exp(-(p_1 s_1 + p_2 s_2 + p_3 s_3 + \dots + p_x s_x)) \quad \text{Eq 2. 1}$$

Where $I(s)$ is the attenuated energy after leaving the volume, I_0 the original energy of the ray, p_i the linear attenuation coefficient for the corresponding voxel material, s_i the corresponding distance from the ray entrance point to the ray exiting position of the voxel. In medical data the material type corresponds of course to the different tissue type. For detailed description of the optical model of the X-ray please refer to [Max95].

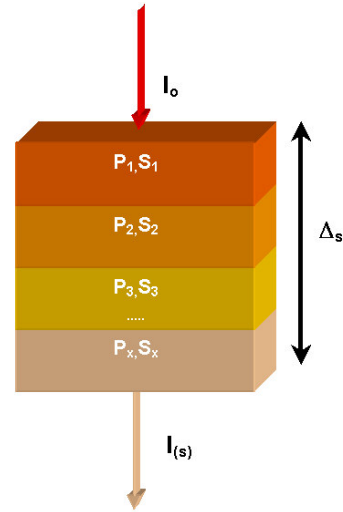


Figure 2-8. Attenuation of original ray energy I_0 to $I(s)$ through a sequence of materials.

The contrast intensity of the final DRR image on the screen level can be calculated using the equation:

$$I_p = I_0 * (1 - L) + I_{background} * L \quad \text{Eq 2. 2}$$

With L representing $L = \exp(-(p_1s_1 + p_2s_2 + p_3s_3 + \dots + p_x s_x))$

To simulate with accuracy the real concept of the X-ray optical model is a complicated task. The main reasons are that the X-ray photon absorption is related to the material properties and the energy of the ray. Basically there are two physical phenomena that occur during ray interaction with the material:

1. **The photoelectric phenomenon.** During this process the energy of the X-ray photon is completely absorbed from the material, irritating an electron on a specific orbit by giving to it more energy, to jump to new orbit with higher energy. After a very small time phase dt the electron returns back to its old orbit emitting a photon. This principle corresponds to an optical model with absorption.
2. **The Compton phenomenon.** This process occurs when the energy of the X-ray photon is higher than any corresponding energy an electron of the specific material can accept. The result is either emission of a new photon from the material or scattering of the current travelling photon of the X-ray beam to a different direction.

In diagnostic X-ray imaging, the X-ray generators produce a spectrum with multiple photons energies. As a result the low energies are absorbed very quickly when travelling through the material, loading with low energy, but not wanted, dose the subject under examination. High-energy rays are responsible for the Compton effect that produces artifacts in the image quality, usually blurring. So the “good” energies that are responsible for generating high image quality are those that are completely absorbed from the material. During simulation of the X-ray model all authors use ray with single energies. This simplifies significantly the model and also avoids the artifacts spectra X-ray energy produces.

To reconstruct a DRR the digital CT data of the patient are used. There are also researchers that try to reconstruct DRR images from MR data [Rams98]. However our focus is on the contrast quality of the DRR image using CT data. Each voxel acquired using CT has an value that is called the Hounsfield unit upon the name of the father CT. The HU can be estimated using the following formula:

$$HU = \frac{(\rho_{\mu} - \rho_{water})}{\rho_{water}} * 1000 \quad \text{Eq 2. 3}$$

Where ρ_{μ} , ρ_{water} are the attenuation coefficient of the material for the specific voxel and the water respectively. When on the above equation one replaces the $\rho_{\mu} = \rho_{water}$, then will receive a $HU_{water} = 0$. In addition the *air* as material corresponds to $-1000HU$, since $\rho_{air} = 0$. The Hounsfield units have no upper limit but usually for medical scanners a range between -1024 to $+3071$ is provided. Apparently 4096 different HU values are provided and therefore to illustrate the complete range of the HU on a volume 12bit voxels are required. It is common understanding that in order to simulate the DRR using CT data the Eq 2. 3 must be used to find the ρ_{μ} of the corresponding tissue.

Imaging with CT offers a great advantage against the conventional radiographs [Kalen01]. Although both imaging methods, radiograph and CT, use X-rays, they provide

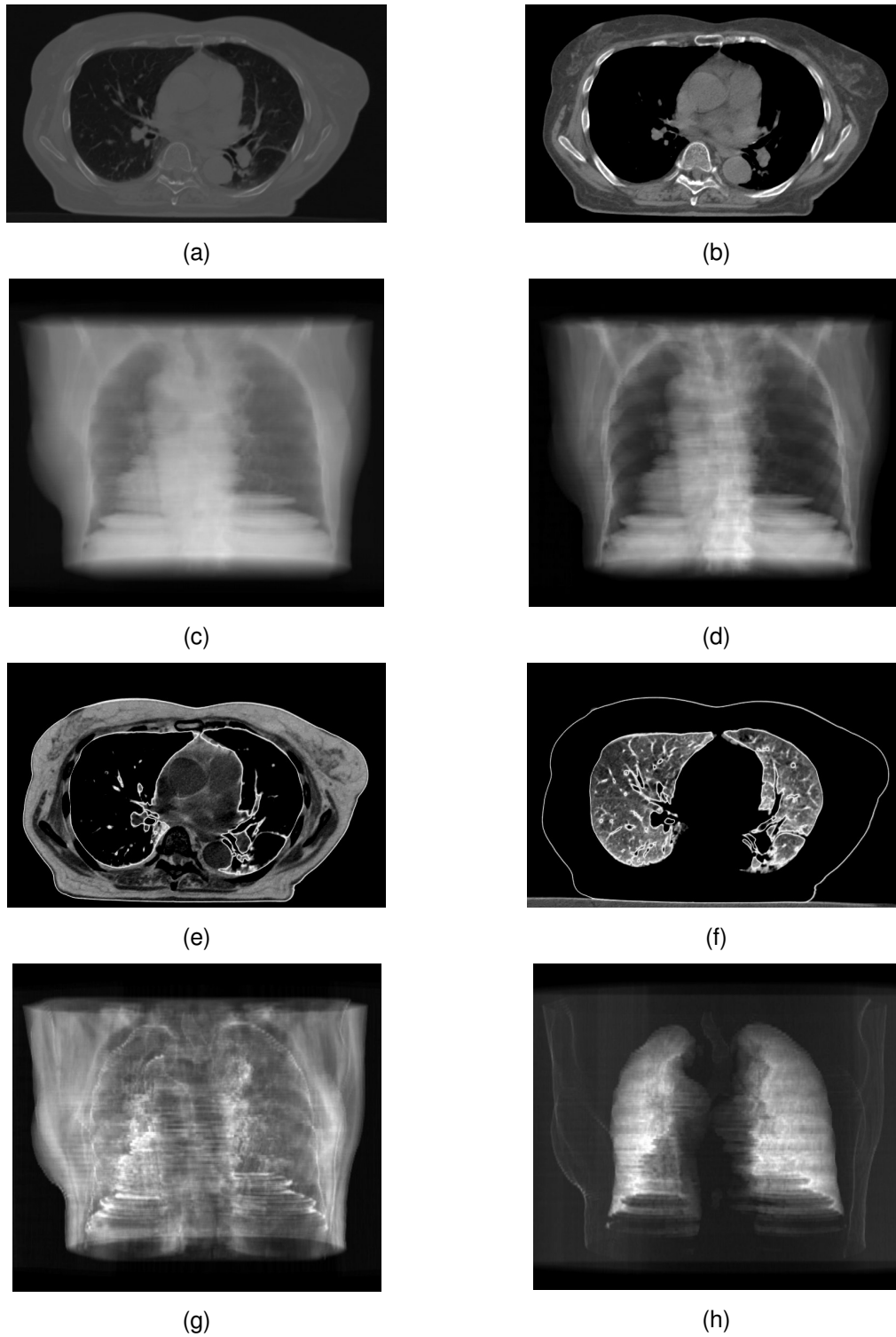


Figure 2-9. DRR reconstruction of CT chest volume. The results are produced using manually manipulated transfer functions. One can observe the corresponding 2D contrast effect on the CT slices in (a), (b), (e), (f).

information about different quantities. Basically in conventional radiograph each picture element displays the integral of the attenuation components along a line, superimposing all visited structures along the ray. On the other hand contrast in CT imaging is determined locally, by the composition of the tissues, while neighbouring structures have no or little influence to the final contrast. Since the CT values have a wide range it is necessary to use also a similar range of grey value for displaying. However, human observers can see up to 60 or 80 different grey levels. To improve the contrast of a CT image, a contrast enhances technique known as image windowing is usually applied on the original range of the HUs in means of look-up-table (LUT) affecting only the final, displayed values [Kalen01]. The most common type of image window is known as the linear ramp window. The basic features of this window are its upper and lower limit and its centre. Values that are below the lower limit will be displayed with black colour and values above the upper limit will be displayed with white colour. One can generate several types of image windows, like non linear, broken and so on.

Assuming now that one uses the accumulation model described in Eq 2.1. The final reconstructed image will be suffer from poor contrast due to the following reasons:

- a) The high range of the HU that manipulated to their complete range and
- b) The superimposing of all HU along the line, since the same principle is used as in the conventional radiography. This issue cannot be avoided due to the principle of the model we want to simulate.

What can be improved is the tissue range selection from the complete volume, in order to increase the contrast of the final reconstructed image, similar to the 2D image display. In this case the range selection LUT will have the same result as on the 2D image. Figure 2-7, illustrates the effect how the most simple LUT used for displaying 2D CT images can be applied on reconstructing 3D DRRs. When applying such value mapping tables in volume reconstruction we use the term transfer function (TF). Images from (a) to (d) have been generated using the ramp LUT/TF. Images from (e) to (h) have been generated using a tent LUT/TF. Important to notice images (a) and (c) since they have been generated with the original distribution of the HU. In other words no HU range selection has been given. For the sake of completeness the next paragraphs will present the most popular technique to generate transfer functions in direct volume rendering and especially in the application field of radiation therapy.

Several researchers reported ways to generate transfer functions for direct volume rendering but not specifically for DRR. He *et al* [HeHoK96] proposed a method where the search of the transfer function was treated as parameter optimisation problem and was addressed with stochastic search techniques. Their approach generated a number of transfer function for the user avoiding the user to perform the same process using the “trail and error” approach. Fang *et al* [FangB98] define a model for generating transfer functions as sequence of 3D image processing procedures. The user had to adjust a number of qualitative and descriptive to achieve their visualisation goal. The freeform design of transfer functions has the advantage that the user can manipulate any of their parameter to get a final result. The drawback of these methods is that it is difficult to be evaluated and accepted in the daily clinical routine. An intuitive way for TF specification from weighted component functions is presented in [Castr98]. A small number of parameters is used, which is sufficient to completely describe a TF. The user is the one who con-

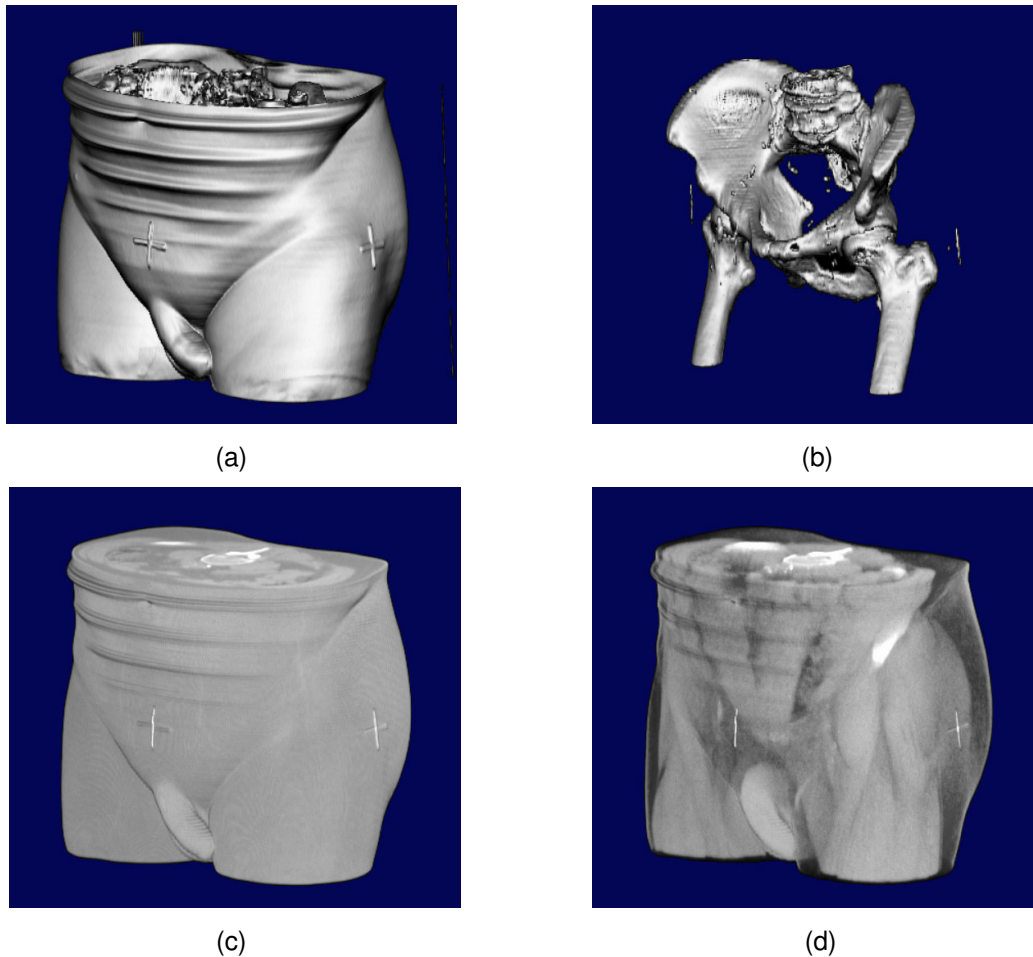


Figure 2-10. Direct volume surface reconstruction. In (a) & (b) reconstruction of volume surface using auxiliary gradient volume estimation [Levoy88]. In (c) & (d) direct surface reconstruction based only on colour and opacity TF.

controls the parameters according to the dataset used defined a specification scheme for semi-automatic TF search techniques.

Galvin *et al* [Galvi95] presented the use of DRR in treatment planning and CT simulation. They reconstruct DRR images using freeform transfer functions and generate unique images that could not be produced with conventional radiography. Adapting similar thinking Cai *et al* [Cai99] presented a method for creating transfer functions for the reconstruction of DRR. He mainly focused on the continuity of the transfer function, especially when sampling at the boundaries of two materials. The realised method could generate a partially composed transfer function for reconstructing DRRs, considering the continuity between different tissue types. He investigated the two types of continuities the linear (C^0) and cubic (C^1). Advantages of these methods are the smoothness of the final image and the flexibility to modify the attenuation coefficients for each tissue type as well as the appearance of specific tissue in the final image result. These features make this approach most convenient and optimal for clinical routine.

Killoran *et al* [Killo01], try to optimise the contrast of the chest DRR using as guide the traditional radiograph. Their aim was to resemble traditional radiograph of the chest en-

hancing similar structures the traditional X-ray image does. This approach gave good results on chest DRR, but restricted the visualisation capabilities on producing to specific type of images, since two 2D images had to be produced and then merged on a different step.

2.3.1.2 Surface reconstruction

Generally there are two methods for reconstructing surfaces: the polygon based and the voxel based techniques. Polygon based techniques can be further subdivided into those methods that generate triangles from planar contours [Boiss88], [Geige93], [Payne94], [Bajaj95], those that generate polygon surfaces iso-values from a discrete scalar field [Loren87], those that reconstruct surfaces from arbitrary 3D points [Hoppe92], [Ament98] and to those methods that use polynomial functions to optimally match the shape of the geometric object they want to represent [Kobbe98], [Morse01], [Carr01], [Turk02]. In medical imaging usually we deal with volume data and thus it is very common to use voxel-based techniques to reconstruct the surface of anatomical structures. The basic idea on these techniques is to determine the edges of the anatomical structures is usually the thresholding through a TF or combined with the opacity volume (gradient or iso-value modes). In both cases the data values are mapped directly to the rendering image.

Probably the most common methods for reconstructing surfaces directly from voxels are the gradient surface and iso-surface model. This rendering model is widely used in almost all medical data sets to render the surface detected by the gradient operator. Levoy *et al.* presented this concept [Levoy88], which is effectively used in most medical imaging applications for the last decade. The opacity calculated by the TF is blended in the final pixel with the local surface illumination model. An example of that method is presented in Figure 2-10 (a) & (b). Another aspect of voxel-based surface rendering is the use of TF. By using transfer functions one can assign optical properties to the original data values, like opacity and colour [Sabel88], [Drebi88], [Höhne90]. The final rendering result is directly affected from the selection of the transfer function. This involves the regions that will be visualized as well as the quality especially at the boundaries of the structures (see Figure 2-10 (c) & (d)).

2.3.2 Radiation Beam Arrangement and Visualization

Conventionally the RT verification process is based on external landmarks, manual drawing of the irradiation field on the patient's skin and portal image verification using high energy X-ray. The external landmarks are marked on the patient during real simulation as indicators of the projection of the radiation beam. This projection involves very often, delineated field shapes according to the radiation blocks that are used for protecting the healthy structures. A necessary tool in 3D-Sim and generally in treatment planning is the 3D projection of the shape of the radiation field and its virtual light together with the CT volume data. This tool increases the physician's ability to appreciate the 3D shape geometry and orientation of the radiation field in the space, a tool that is not available on the physical simulator. Additionally the light field projection of the patient's skin is used as the standard verification tool for the field arrangement. In this work our concern is the real time projection of the radiation polygon geometry and its projection on the surfaces of the CT data. To achieve this we use a convex polygon scan conversion algorithm combined with the Z-buffer information provided from the 3D rendered image. In this work we do not aim to present a new polygon-volume hybrid rendering reconstruction scheme. Instead a

solution to the problem of real-time and accurate treatment light field illustration is shown. For more information on the hybrid rendering concept the reader can refer to [Levoy90], [LevoB90] and [Bhale00].

2.3.2.1 Polygon Scan Conversion

To realize the features mentioned above we employ a hybrid volume rendering approach. Our method is based on a 3D triangle polygon scan conversion (PSC) and contributes on the rendering scheme on the image level. Detail information about similar algorithms can be found in [Gordo94], [Encar96]. In this work our focus is to describe the combination of the PSC approach with the Z-buffer in order to produce the wanted results. In order to achieve our aim first the beam polygon is constructed. Since our PSC method can be applied only on convex objects, every polygon object used in the rendering scene must be a tetrahedral (product of triangles). To represent in 3D the radiation field we consider the 2D radiation field size. Basically a pyramid is generated that corresponds to the perspective of the radiation field. This shape is composed from six triangles, four compose each side of the pyramid and two triangles its rectangular base. In relation to the physical parameters the high of the pyramid represents the source to detector distance and the size of the pyramid the actual field size scaled at the perspective factor. Before processing the polygons that compose the field for the scan conversion algorithm, we apply to them homogeneous coordinate transformation means of matrix form in order to match the CT volume geometry and to register the virtual simulator parameters of the planning components (gantry and couch). The next step will be the hither clipping against the 3D image

For the polygon reconstruction follows the generation of the data structures. The necessary data structures for realizing the PSC are:

1. The edge list $P_i(x, y, z)$ (EDGE). This list hosts the actual vertex information from every 3D polygon.
2. The sorted edge list (SEL). This list is generated after sorting the list of EDGE's in top-to-bottom y order of the first vertex.
3. The active edge list (AEL). The active edge list is the current polygon edge list that will be scanned.

The main body of the algorithm, passes iteratively loops through the SEL and then through the AEL. Aim of the scan conversion is to generate a semi-transparent effect of the radiation field polygon so as to allow the viewer to see the surface of the structures behind the radiation field and also to indicate-highlight the field intersection volume with the patient volume. Both tasks should be accomplished at the same step. To achieve that we calculate the Z-depth of the polygon side during scan conversion and we compare the estimated value with the current Z-depth of the surface volume. Of course this step assumes that for the current 3D reconstructed image a Z-depth have been calculated. This means that the proposed method can be applied only when the surface location of the volumetric structure is known.

Figure 2-11 illustrates this principle in a simplified 2D case. We assume that the 3D scheme is viewed from the top and the viewer, the 2D image plane, is located on the left of the image. Let us consider three different Z-depth values for an arbitrary edge of the polygon with $Z_{p_{10}} < Z_{p_4} < Z_{p_1}$. One can very easily understand that the observer from the image plane will be able to see the polygon object at the levels Z_{p_1} and $Z_{p_{10}}$. The pixel value

I_4 will contain information only from the volume surface since the depth value Zp_4 is smaller than the Z-depth Zv_2 of the surface. In a similar manner every polygon is scanned and its depth value is compared with the corresponding surface Z-depth. The colour value for the corresponding triangle position is weighted with the optical depth of the 3D scene in order to more accurately indicate the beam pyramid location in the space relative to the observer and the CT volume. Finally the pixel colour at the position $I(x, y)$, will be composed from the colour of the 3D image pixel $Iv(x, y)$ and the colour polygon pixel $Ip(x, y)$ using a linear blending function.

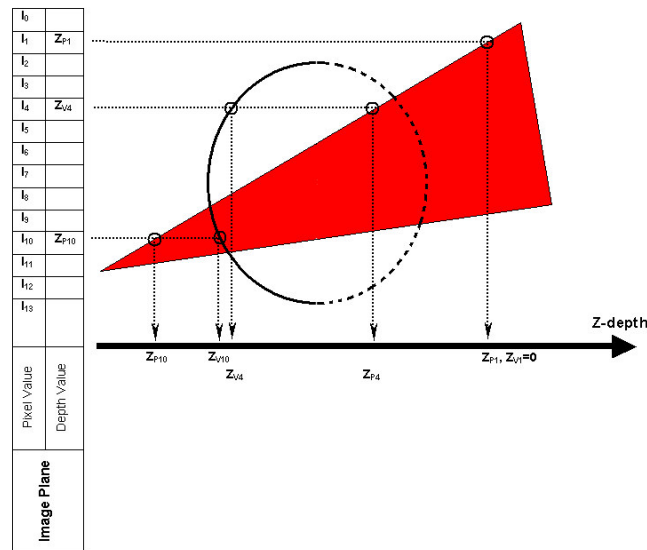


Figure 2-11. Simplified Z-depth estimation during polygon scan conversion. The red triangle indicates the treatment beam polygon and the ellipse the CT data.

The above polygon reconstruction principle can be applied with success on rectangular field shapes, symmetric or asymmetric. In case that more than one fields are involved in the visualization scheme the PSC is applied iteratively for every beam polygon. Figure 5.12(a) presents visualization examples of the above process. To reconstruct more complicated polygon objects involved in the field delineation, a different approach must be followed during polygon generation. It is common one to generate a shielding block in terms of a 2D contour on the DRR. Prior to scan conversion the 2D contour shape must be projected of the 2D DRR image space to the volume space in order to generate the corresponding 3D polygons with perspective geometry. This contour shape can be arbitrary and its convexity varies. Since the PSC algorithm we use can handle only convex polygons, we have to triangulate the 2D contour in order to maintain convexity of the polygon. This step is performed using the two-dimensional Delaunay. Once the 2D block contour is triangulated we must estimate its projection to the virtual detector level. This process will generate equal number of tetrahedral as the original 2D triangles. The scan conversion process is then applied for each tetrahedral object, as performed with the radiation field pyramid.

2.3.2.2 Projection of the Virtual Light Field

A significant aspect for the verification of the radiation field is the virtual light field projection on the patient skin [LuH99]. In physical simulators, a light source is located near the irradiation source. The orientation of the light intensity is diverted through the gantry head using a mirror aperture. The outcome of this process is the exact projection of the radiation field on the patient's skin. The two main axis of the field are indicated as line shadows. In case the radiation field is delineated using shielding blocks, then the light field area is also modified accordingly. This process described above should be performed in a similar manner in the virtual simulation process. In order to realise this principle we take

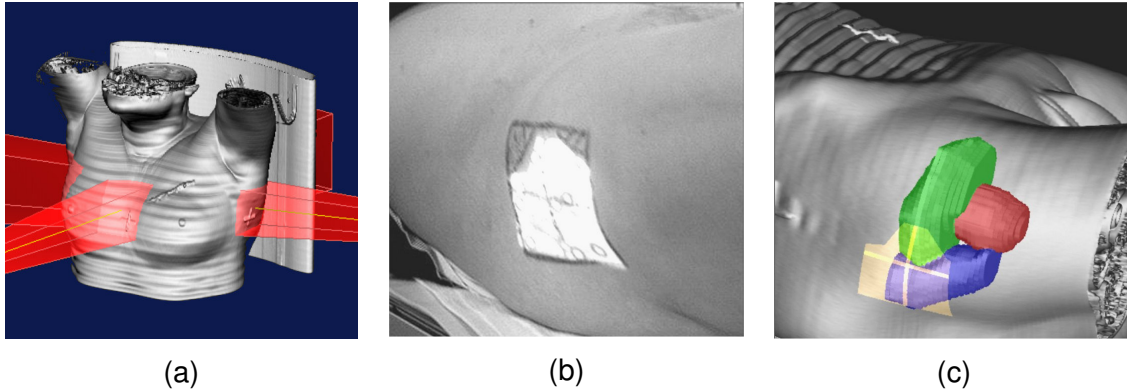


Figure 2-12. Projection of treatment field with patient anatomy. In (a) reconstruction of polygon treatment fields. In (b) a real treatment case of a prostate case. In (c) the simulated case of the same patient with the volumes of interest segmented and the virtual light field projected on the 3D reconstructed surface.

advantage of the convexity of the tetrahedral objects and the Z-depth information derived during polygon scan conversion.

For simplicity let us consider a 2D example. Assume that the back edge, in relation to the object position, is currently under scanning. We use a 2D image that has the same size as the reconstructed one, in order to indicate that the corresponding pixel has been visited during polygon scanning process. We will call this array light mask. At this step we introduce the values Z-buffer $Z_V(i,j)$ as they are acquired during the volume rendering process. If one compares the current edge Z-depth $Z_P(i,j)$ with the value of the image Z-buffer then could make the following two assumptions:

- if $Z_P(i,j) < Z_V(i,j)$ then the current polygon edge is behind the volume and is hidden from the viewer. In this case no value for the light mask is accumulated.
- if $Z_P(i,j) > Z_V(i,j)$ then the current polygon edge is in the front of the volume and is visible from the viewer. In this case one value for the light mask is accumulated.

It is known that the polygon objects we use during scan conversion are convex. In case all polygons are scanned without any object to obstruct the back polygon, then there will be only two indices for each pixel that was visited during polygon scanning. Two are the maximum number of indices we can achieve on the light mask. Considering the viewing location, at the level where the beam polygon intersects the volume surface the light mask goes from value two to one. This means that all pixels in the light mask that have index one should be considered as the projection of the light field. The virtual light field follows every orientation of the radiation beam, including any modification in one of the parameters gantry, collimator or couch. Mixing of the volume surface information and the light mask information occurs similar to the polygon projection on the image level. The corresponding pixel colour of the 3D image will be modified at those locations when the light mask is indexed with value one.

To generate the visual effect of the delineated radiation field in cases where shielding blocks are used, we use a second 2D array, similar to light mask, named block mask. The block mask is filled using exactly the same principle with the Z-depth values of the polygon edges and the volume surface described above. In case that the block mask is marked with zero index then the block polygon is hidden from the volume. Index one in

the block mask means that one polygon edge is hidden from the volume and the other one is visible hence an intersection of the block polygon with the volume surface exists. If the block mask is flagged with two indices then both planes of the block polygon are closer to the user than the volume surface. To produce the final image we combine the two masks accumulated above, the light mask and the block mask. Pixels regions that overlap and have common values, index one and two, are omitted during image shading. A clinical example of a real prostate light field projection is shown in Figure 5.12(b). The corresponding virtual light field is shown in Figure 5.12(c). Further clinical examples and the clinical importance of this method can be found in [Zambo02] and [Houston02]. Our approach for visualizing treatment beam polygons and light field projection offers a significant speed advantage when displaying the treatment fields on 2D slice and on 3D. This property is very important when the user changes the orientation and the size of the field, or when applies fine-tuning of the block or MLC shapes. In this case we are able to display in real time the modifications that occur on the 2D and 3D field projection. This way one can focus on a specific anatomical location and can observe the field adjustments in relation to that point.

2.3.3 Room View

The conventional simulation and treatment procedure are taking place in specialized sites where the observation of the real hardware machine and the patient location on the couch of the treatment device should be available (see Figure 2-13). The treatment rooms are always monitored with external cameras in order to assure maximum secure and protection for the patients and of course the working personnel. General causes for accidents in daily routine are unpredictable. However the most potential reasons for accidents are usually collision between mechanical components or even between components and the patient under treatment. Also misalignment in patient setup (e.g. wrong patient orientation) or inaccurate submission of the treatment parameters might result to a long-term but severe injury of patient's vital organs. In clinical routine most of the treatment cases must be planned through a TP or a VS system. Currently in 3D conformal treatment planning, semi-automatic and automatic techniques for beam placement have been introduced, in order to improve treatment outcome. These techniques result to a large number of beams with complex arrangement. It is often the case that complicated techniques cannot be applied on the treatment machine due to prospective mechanical collision or due to interference of metal components in the irradiation field.

The above reasons advocate the demand of a graphical simulation tool of the clinical room environment in the TP and VS systems. The first overview came from Sherouse [Shero91] who reconstructed a very simple 3D model of the treatment machine in order to provide visual feedback of the machine configuration (gantry and couch). The graphical model of the treatment machine was updated accordingly after a treatment pa-

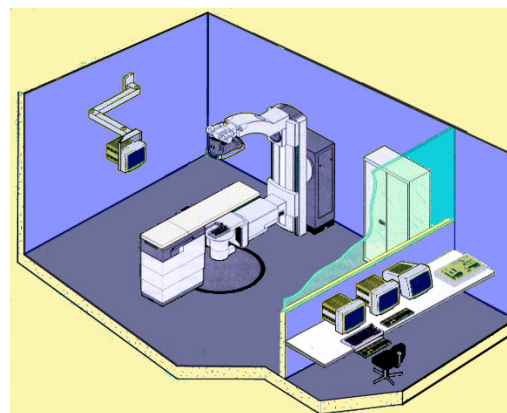


Figure 2-13. Graphical representation of the conventional simulator environment.

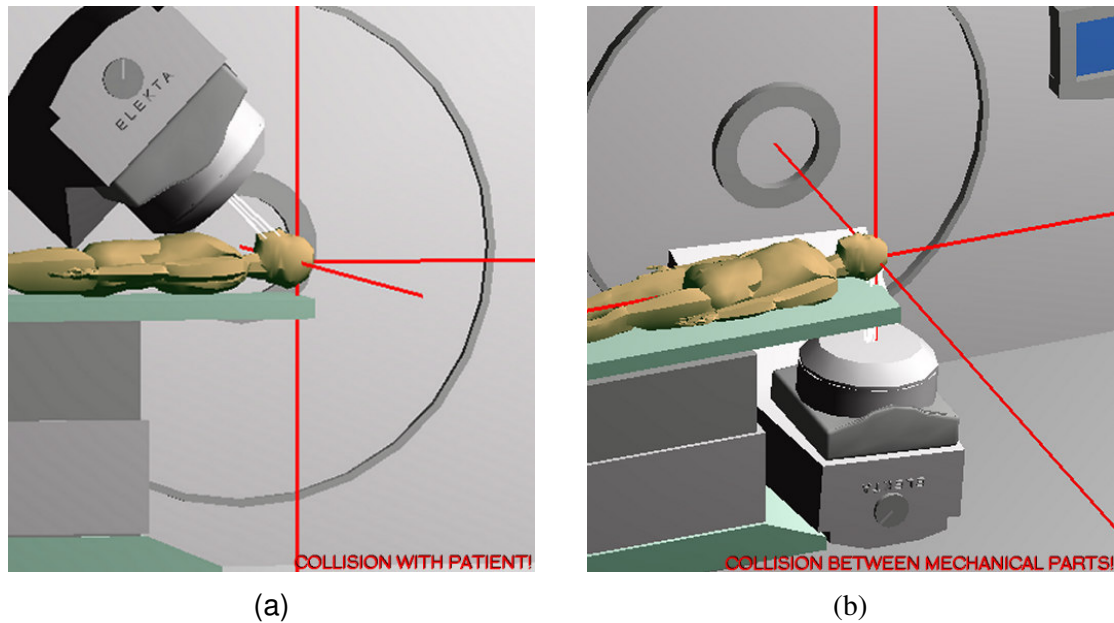


Figure 2-14. Indication of potential collisions during RT treatment using ARIS. A potential collision between patient and mechanical parts is shown in (a). Similarly (b) shows a collision between mechanical components of the Linac.

parameter was modified. The term Room View (RV) was introduced from Purdy *et al* [Purdy93]. However that term was used to describe the 3D view the patient's body contour and internal organs. The RV was reconstructed using polygons and contour lines and provided interactivity to the user in order to observe beam interaction with the patient body, critical organs and target volume in three dimensions. In this work, we will refer with the term RV or "room's eye view" (REV) to the representation of the treatment machine's room with or without the model of the patient.

Realistic and functional modelling of the treatment machine and its components is reported from several authors. Among the most important was Humm *et al.* [Humm95] who introduced an application for collision avoidance using the REV. The treatment machine and the patient's body, were reconstructed using polygon surface rendering compiled by the OpenGL, graphics language. A phantom model, reconstructed from the corresponding CT data, replaced the patient's body anatomy, located on an arbitrary position on the treatment machine's couch. This collision detection approach could provide the planner with an immediate feedback of the feasibility of each field during treatment set-up. If a potential collision was detected then either the couch configuration was remedied or the closest allowed gantry angle was calculated and used replacing the old one that result to collision.

In the content of computer-controlled systems, which is used to apply the current treatment set-up to the treatment machine, Kessle *et al* [Kessl95] presented a software application for controlling the treatment machine including its exact polygon representation. Characteristic of this approach was the use of an "icon-based treatment script manager". Each icon represented the configuration steps that the treatment machine should follow in order to reach the final field orientation. The collision detection was applied in every step of the sequence. In case of detected collision on a specific step, the script

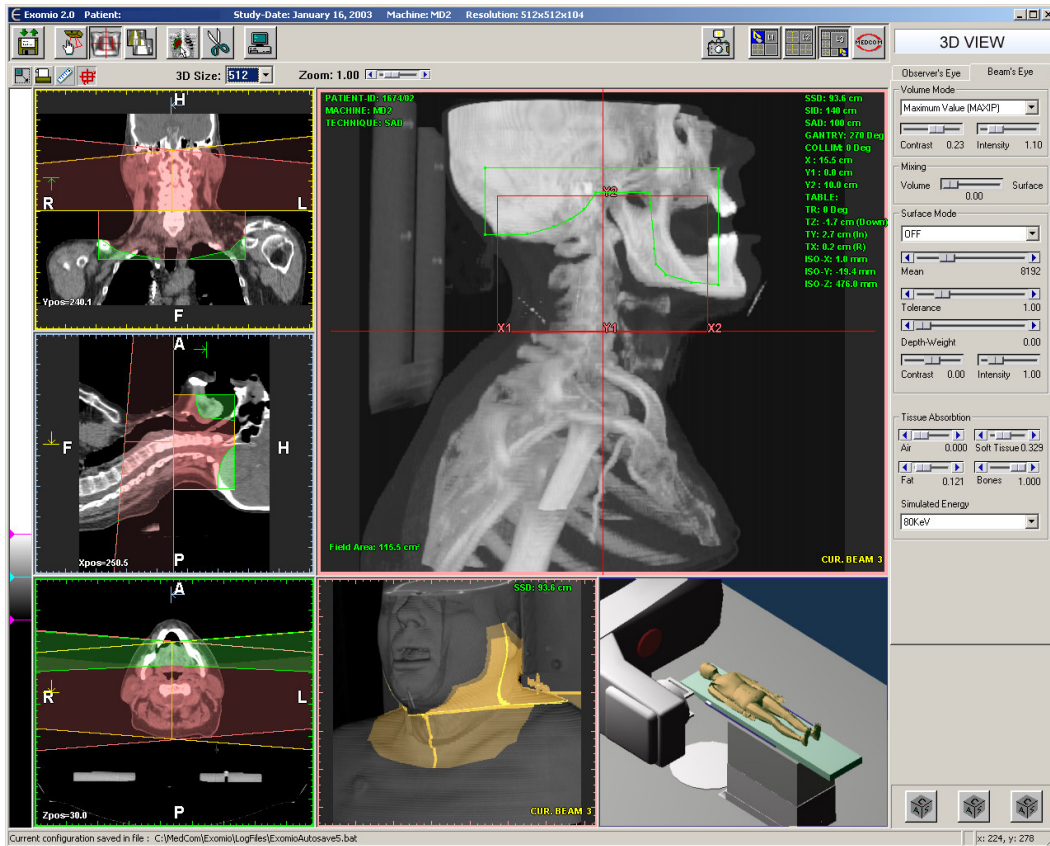


Figure 2-15. A representation of the 3D-Simulator (Exomio). On the left side of the screen is shown the representation of the original and reconstructed CT slices (top-coronal, middle-sagittal, lower left-axial). Beam and block overlay are present over the neck region. On the top right window a MIP reconstruction of the BEV. The OEV with the three light field projections is presented on the lower middle window. Finally a realistic representation of the treatment unit (LiNAC) as provided using the ARIS visualization engine is shown on the lower right image.

manager was used to modify the sequence of the icons, rearranging the order of the icon-steps resulting to the correct sequence. This approach could provide an excellent feedback to the user about each step of the treatment set-up. Only drawback of this approach was the lack of the model of the patient's body.

Tsiakalos *et al* [Tsiak01] also presented an approach for automatic collision detection in the conformal and stereo tactic radiotherapy treatment planning using the REV. The treatment machine was reconstructed with exact geometry using the OpenGL graphical library. An average model of the patient was used as an approximation of the patient's body anatomy. However the user has the option to modify the size of the patient model in all three dimensions. To detect the collision between polygon structures the Coldet library was used. By detection of a collision a warning indication was appeared describing the type of the collision (e.g. collision between couch and gantry). The greatest advantages of this approach are:

1. The simplicity of modelling any treatment machine geometry and their external components if any.

2. Easily incorporated to any 3D-Sim or TP system.

The above reasons support this approach as the most potential solution for integration into an already established software environment of a 3D-Sim system. An example of the system is given Figure 2-14 where a model of the Elekta treatment machine is illustrated simulating two potential collisions.

2.4 Summary

This chapter provides an overview of the most important component of the conventional simulator and the 3D-Sim. We consider this as necessary step in order to appreciate these two different concepts. For the conventional Simulator we formulate the most important mechanical and practical limitations. On the other hand we presented the alternative solution to the conventional Simulator that is the 3D-Sim concept, which is a software system composed of several graphics and visualization tools.

Input to the system are 3D data from medical imaging modalities and especially data coming from CT. Without questioning the “heart” of a 3D-Sim system is the volume-rendering engine. Volume rendering allows the system to reconstruct DRR and surface images of the patient anatomy. Compared to standard X-rays in DRRs one can manipulate the tissue weight and contribution to the final image producing interesting and unique information. In a similar manner volume surface images can be reconstructed with user defined TF.

Essential visualization component is the 2D and 3D the display of the treatment field in relation to the patient anatomy. Further more the display of the virtual light field can be used as verification for comparing digital results produced in the 3D-Sim system and the real world, before patient treatment. Finally incorporation of a collision detection solution in the 3D-Sim environments, using the real LiNAC geometry for modelling, allows the evaluation of the plan applicability before further treatment actions are taken. An illustration of the *Exomio* 3D-Simulator software is shown in Figure 2-15.

Chapter 3

Segmentation of Anatomical Structures: Manual volume definition and semi-automatic extraction of the spinal cord

3.1 Introduction

Segmentation is the process that separates an image into its important features (primitives) so that each of them can be addressed separately. This converts the planar pixel of the image into a distinguishable number of individual organs or tumour that can be clearly identified and manipulated. The segmentation process might involve complicate structures and in this case usually only an expert can perform the task of the identification manually on a slice-by-slice base. Humans can perform this task using complex analysis of shape, intensity, position, texture, and proximity to surrounding structures. Of course, all these features are differently qualified depending on the experience of the user. To perform a similar procedure automatically using a computer since today has been proved a very difficult task. In other cases where simpler anatomical regions with a very distinguishable shape must be identified an algorithm can perform this task. Currently there are only dedicated algorithms for different regions of the human body. To generate a “complete”, with a general meaning of the term, segmentation application numerous tools and algorithms must be combined [Kuszy95].

We will investigate the volume segmentation aspects within the frame of radiation therapy. From the engineering point of view volume definition seems probably to be a simple and straightforward line drawing process. However, from the clinical point of view, it is a very serious task. The clinicians consider this action as more than line drawing, since this process will define the precise borders between disease and healthy tissues. The first aim of the segmentation process in RTP is to define as accurately as possible the target that will be irradiated. This process is a manual process and usually is performed from an expert oncologist. With the terms of manual process, we mean that the physicians will exam the digital volume, slice-by-slices and using the mouse cursor will illustrate the shape of the tumour. The coordinates of the shape of the tumour are stored from the system for further processing. The target definition process is probably the most time consuming process involving an expert during the RT planning [Ketti97]. It would be almost impossible to perform the same process using a computer. The following describes a number of reasons proving that the automatic target volume definition is still very difficult to be performed from an expert system. The obvious reasons found in the daily clinical routine are:

1. The irregular tumour properties, like shape, texture, volume, relation with surrounding regions.
2. Location within the human body. A tumour theoretically could grow anywhere within the patient's body. There are cases where the disease statistically appears

on common organs like prostate to males and mamma to females. In these cases, a region-based automated segmentation process could probably be suitable for solving the problem.

3. Tumour spreading and variation. Depending from the region the tumour is grown, disease cells might spread to the surrounding region. The disease cell distribution cannot be predicted and detected on the digital patient's data. Since the internal organs in the human body perform several vital processes are active very often their moving. A very common example is the prostate variations since the bladder change its volume very easy and the rectum contracts [Dawso98], and abdominal and lung tumours that vary according to patient respiration [Aruga00].
4. Artifacts in the acquired digital data. When treating elderly patients it is often the case to have prosthesis, usually metallic (heart irritating) like hip prosthesis. These patients cannot be examined in a MRI modality and therefore CT imaging is the only alternative for their RTP. Nevertheless, it is well known that metallic components generate severe artifacts in CT imaging that reduce image quality and blur tumour borders.

Further, the physicians must follow a number of regulations determined by international committees in RTP [Purdy96]. Nowadays several 3D RTP and 3D-Simulation systems are available and are widely used in most of the oncology clinics throughout the world. These systems have such planning capability, that leads to new treatment techniques, which in many cases are much more complex than the traditional methods like IMRT that irradiate the tumour cells with higher dose rates. Thus, the accurate manual target volume definition is even more necessary nowadays. So far only a very few techniques propose physicians one or more alternatives for volume definition [Ketti97], [Belsh97]. Recently Pekar *et. al.* [Pekar04] reported a method based on an adaptation of 3D deformable surface models to the boundaries of the anatomic structures of interest. The adaptation was based on a tradeoff between deformations of the model induced by its attraction to certain image features and the shape integrity of the model. Nevertheless, to make the concept clinically feasible, interactive tools were also introduced that allow quick correction in problematic areas in which the automated model adaptation may fail.

In the following paragraphs, we will discuss a unique contour interpolation method that can accelerate and improve the quality of the manual segmentation process of tumours and other normal structures. The algorithm is based on a fully 3D interpolation scheme given the user all possible flexibility during segmentation. Considering spine as an organ of high importance that has to be protected during patient treatment, in the last paragraphs of this chapter we present a semi-automatic method for extracting the spine volume with high accuracy.

3.2 Manual Definition of Structures

The manual definition of structures is a process that requires the intervention of an expert in order to define the shape of a structure, usually tumour or disease growth. Traditionally in most applications, this process takes place in the original acquired image. Since here the focus is on the CT modality, the indicated image direction is the axial. The CT images are collected on a plane that has its normal vector moving parallel to the longitudinal axis of the CT table and therefore longitudinal of the patient as well. Image quality is and will always be a very important factor for the accurate definition of anatomical structures.

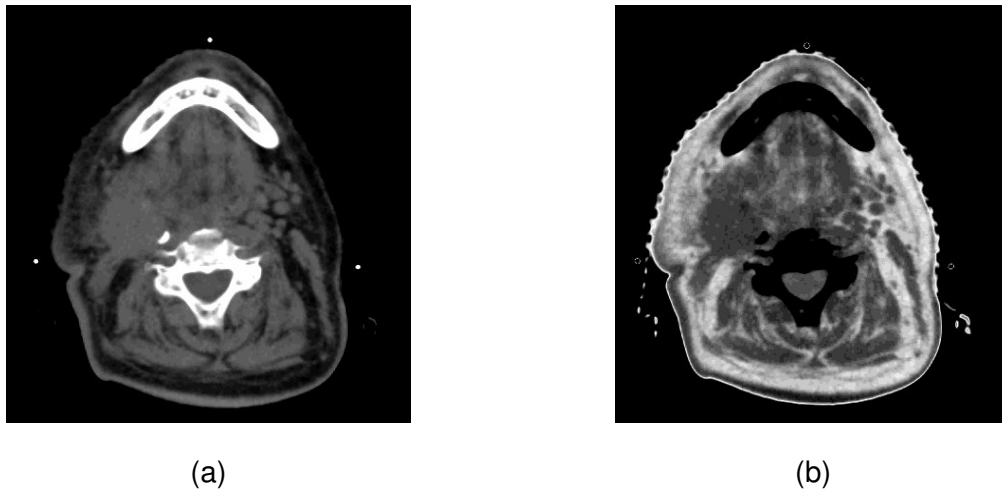


Figure 3-1. Illustration of CT slices using different windowing functions. In (a) contrast adjustment using standard linear ramp function. In (b) a rather unusual contrast set-up for radiotherapy, using linear triangle function.

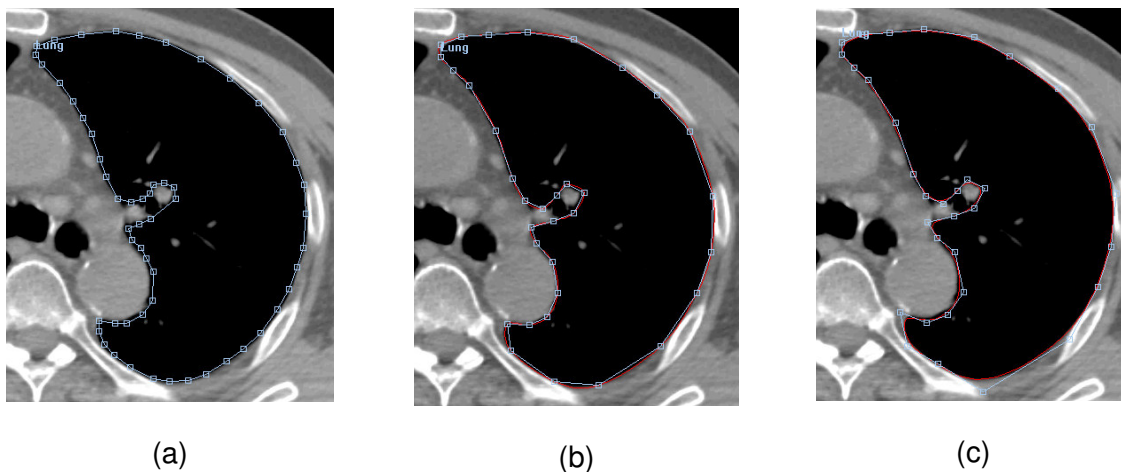


Figure 3-2. Manual segmentation of the left lung region. In (a) linear interpolation is used to connect the 56 key points defined from the user. In (b) the same contour but with smoother shape is interpolated using cubic interpolation and half of the points needed in (a). Similar in (c) where B-Spline interpolation is used.

Even the set-up of different image contrast and intensity (image windowing) might affect the decision making during volume definition. Image grey level enhancement is related with the:

- Improved illustrations of the edges, which be broaden or narrow depending on the windowing function used
- Improved display of the wanted structure and the surrounding tissues

Figure 3-1 shows an example of a tumour case in the lymph nodes of the neck region. The contrast of the image on the left side has been adjusted using the standard ramp window. The right image is shown using a triangular window. One can observe the tumour

shape and the small structures better on the right images since the lower intensity structures at the background have brighter colour. Further more simple issues as the line thickness during volume segmentation can indicate user uncertainty and in general can characterize the accuracy of the segmentation process.

Complementary information to the CT data, but essential in many aspects on tumour volume definition is the use of multimodality imaging like MRI [Khoo97], [Rams98] and PET [Maise02], [O'Doh02], [Geets04]. The use of different modalities beyond CT has been proven extremely valuable to investigate tumour shape, size and spread. Usually MR imaging is used to describe better tumours of the brain and cervical regions. As a result, the tumour contrast enhances so as its borders, and that can drastically improve the definition of the target volume. In addition, MRI has the ability to reconstruct anatomical images on different planes like sagittal, coronal or arbitrary planes, where several tumour cases can be clearly illustrated. On the other hand, the use of PET studies provides functional information related to lung tumours. This can result to the detection of tumour spreads and tumour size extension [Caldw03]. Considering this information will eventually assist the improved tumour control. CT is considered as the primary modality for the RTP. Thus the complementary imaging modalities must be fused with CT in order to have the optimum outcome. Several studies exist for volume registration in the frame of RT, that proposed semi-automatic and automatic ways to register different volumes [VanHe94], [Kwa98], [CaiJ99]. In addition, currently technological developments allow the combination of two modalities in one offering automatic matching of the CT and PET information [Beyer00], improving registration accuracy.

Currently the tool used to perform the volume definition is the mouse cursor. The user defines a number of digital points on the image level, closing the first and the last point of the contour to generate this way a structure. The connectivity between the *key points* can be linear or higher order. The higher order connectivity can be achieved using interpolation models like Hermitte cubic, Spline curves, Bezier curves [Laure94], [Spath95], [Cohen01], which are the most common and successfully used techniques for smoothing curves in the CAD systems. Aim of the high order interpolation techniques is to reduce the amount of input points required to describe a smooth shape. This concept can be easily adapted in medicine since most human organs are smooth and round. This thesis does not focus on analysing the properties of the interpolation techniques instead we aim is to indicate the importance of such methods and their advantages. Performing a simple comparison between C^0 order (linear) and higher order interpolation, one can find out that the amount of points used to illustrate the shape of a structure using linear interpolation require at least twice as many samples as by using the higher order interpolation algorithms (see Figure 3-2).

A common methodology used to combine high order interpolation and image edge properties is the use of active contour models. The active contour models or Snakes can be 2D image curves [Kass87], [Blake98] or 3D polygon meshes [Terzo88], which are adjusted from an initial approximation to the image or volume features by a movement caused by simulated forces. Image features provide the so-called external force. An internal tension of the curve resists against highly angled curvatures, which makes the Snakes movement robust against noise. After a starting position is given, the Snake adapts itself to shape by relaxation to the equilibrium of the external force and internal tension. Snakes has been proven efficient and fast for a number of applications in medicine involving different imaging modalities [McIne96], [Gross98], [Behr00], [Sakas01], [Gross02].

3.2.1 Volume Interpolation from Parallel & Non-Parallel Contours

The interpolation techniques described above, are usually applied only on a single slice level (2D). The use of high resolution CT data in 3D-Sim, allows the use of multiplanar reconstructions (MPR) for the sagittal and coronal direction, in relation with the patient anatomy. These two images are orthogonal to each other and perpendicular with the axial plane. The navigation through these images help in the observation of complex anatomy. The sagittal and coronal views often offer a better overview of organs 3D shape. Defining volumes in these directions could be of benefit since several organs are aligned along the longitudinal body axis. Although this can be just a visual trick, since physicians have used to work with X-ray images observing structures in relation with the rest of the anatomy, they consider the multiplanar reconstructed images provide additional information for the shape of the organ. The MPR techniques are used in MRI imaging where the image reconstruction plane can be placed in oblique orientation for the investigation of complex anatomy of brain tumours.

However, there are very few reports illustrating the benefits of the MPR while defining medical volumes. Probably the reason is due to the standards of the imaging modalities, since most of them generate images on a transverse plane to longitudinal direction to the human body. The presented method here is based on the ability to define contours on the two MP directions sagittal and coronal as well. The idea of this tool came from the fact that some anatomical structures cover larger areas when they are visualized on the coronal or sagittal directions. In other words, by defining a contour on a MP image we include several axial images at one step. Now if one can define several contours in the MP images, have created a 3D contoured object. What must be done now is to accurately interpolate the 3D contours and extract a new shape out of them. This approach could accelerate the volume definition process extremely.

The problem we have to solve in our case is the generation of a surface and contours from structured closed parallel and non-parallel contours. The data points represent the contour points as they are generated from the user on the different levels of the axial slices or/and on the MPRs. The most common approaches used to reconstruct surfaces from parallel contours and are well established in medical imaging applications [Boiss88], [Meyer92], [Payne94], [Bajaj95], [Weist00]. The limitation of these algorithms is that they cannot be applied on non-parallel contours. The problem of the non-parallel contours could be also formulated as generation of surfaces from scatter data, which are very common in industrial applications [Hoppe92], [Ament98]. There is a large variation of solution to that problem. Gibson [GibbsM98] extracted smooth surface models treating the existing binary data as a constraining element in an energy minimizing deformable surface system. The resulting data structure can be used either to create Euclidean distance maps for direct volume rendering or employed directly as a polygonal surface model [Gibso98]. Whitaker [Whita00] presented a modified version type of the constrained deformable surface model. His constrained level-set model approach creates smooth models while bypassing the need for separate surface representation. However, while these methods generate smooth surface representations, both the level set model and the surface net remain discretely sampled and retain the problem that they are non-scale invariant.

For our application, we selected the approach presented from Turk [Turk99], [TurkB99]. Their method adapts earlier work on thin plate splines and radial basis inter-

polants to create a new technique in generating implicit surfaces. Their method allows direct specification of a complex surface from sparse, irregular scatter samples. The main restriction of the method is the relatively small number of sample data that can be handled. This drawback makes the above approach unsuitable for a number of applications that a large number of sampling points are needed. The topic of computational complexity by using implicit surface interpolation was addressed by Morse *et. al.* [Morse01]. They explore the method in [Tukr99], applying compactly supported radial basis functions to create an efficient algorithm for computing interpolated surfaces. As a result their technique produces significant improvements in memory utilization and computational efficiency. They used a family of radial basis functions with the necessary continuity but also with compact local support. The result is a sparse system whose solution can be accelerated and the result is single and closed form analytic representation of the desired surface. Yoo *et. al.* [Yoo01] used the approach of compactly supported radial basis functions to reconstruct the surface of the in-vivo bovine aorta from non-parallel, non-uniformly sampled ultrasound slices.

In this work, we demonstrate the use of implicit function interpolation to reconstruct 3D organ shapes from closed planar parallel and non-parallel contours that have been defined selectively by the user. The total number of contour points will be used as the input data to the implicit surface algorithm with arbitrary order. The number of these sampling points will not exceed the level of few hundred, and therefore the calculation times will be in acceptable ranges despite the complexity of the algorithm. The output result of the reconstruction algorithm is provided in two forms: as a triangulated mesh or as multiple parallel contours extracted in arbitrary plane directions. For the RTP applications we focus mostly on the reconstruction of contours in the axial direction. The algorithm can be separated into different modules from the point editing until the reconstruction of the surface and contours as follows:

1. Collection and processing of the given contour points. This step involves the generation of the contour constrains and filtering of unwanted.
2. Calculation of the implicit functions in 3D. In this step the information produced in step one will be used to solve a linear equation system that will provide the coefficients representing our interpolation function.
3. Evaluating the implicit function over a 2D or 3D grid we extract 2D planar contours or 3D polygon meshes respectively.

Before presenting technical details of the algorithms, we first introduce some definitions related to radial basis functions (RBF) and implicit surfaces.

3.2.1.1 Radial Basis Function Approximation

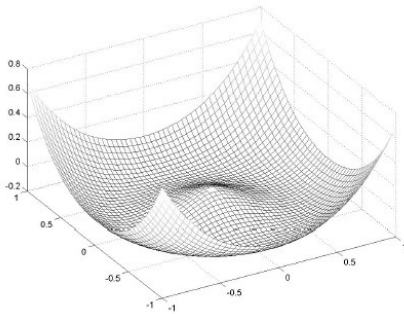
Our approach relies on scattered data interpolation to solve the shape transformation problem. The problem of scattered interpolation is to create a smooth function that passes through a given set of data points. The two-dimensional version of this problem can be stated as follows: Given a collection of k constraint points $\{c_1, c_2, \dots, c_k\}$ that are scattered in the plane, together with scalar height values at each of these points $\{h_1, h_2, \dots, h_k\}$, construct a smooth surface that matches each of these heights at the given

locations. We can think of this solution surface as a scalar-valued function $f(x)$ so that $f(c_i) = h_i$ for $1 \leq i \leq k$.

One common approach to solve scattered data problems is to use variational techniques (from the calculus of variations). This approach begins with an energy that measures the quality of an interpolating function and then finds the single function that matches the given data points and that minimizes this energy measure. For two-dimensional problems, thin-plate interpolation is the variational solution when using the following energy function E :

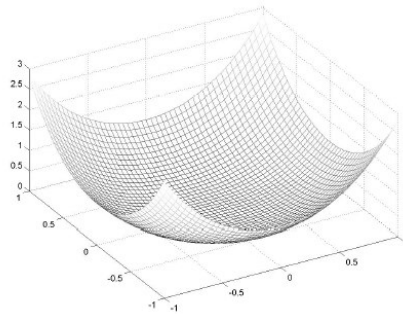
$$E = \int_{\Omega} f_{xx}^2(x) + 2f_{xy}^2(x) + f_{yy}^2(x) \quad \text{Eq 3.1}$$

The notation f_{xx} means the second partial derivative in the $f(x)$ direction, and the other two terms are similar partial derivatives, one of the mixed. The above energy function basically a measure of the aggregate squared curvature of $f(x)$ over the region of interest Ω . Any creases or pinches in a surface will result in a larger value of E . A smooth surface that has no such regions of high curvature will have lower value of E . The thin-plate solution to an interpolation problem is the function $f(x)$ that satisfies all of the constraints and that has the smallest possible value of E .



$$\phi(x) = |x|^2 \lg(|x|)$$

(a)



$$\phi(x) = |x|^3$$

(b)

Figure 3-3. 3D representation of RBFs used in this work. In (a) the biharmonic radial basis function used in 2D interpolation schemes and in (b) the triharmonic radial basis function applied in 3D schemes.

As described in [Turk99], the scattered data interpolation problem can be formulated in any number of dimensions. When the given points c_i are positions in N -dimensions rather than 2D, this is called the N -dimensional scattered data interpolation problem. In this work, we will perform interpolation in three dimensions. When we refer to problems for great than 2D then the term thin-plate is less meaningful. The alternative term used is the variational interpolation and means the generalization of thin-plate techniques to any number of dimensions.

The scattered data interpolation task as formulated above is a variation problem where the desired solution is a function, $f(x)$, that will minimize Eq 3.1 subject to the interpolation constraints $f(c_i) = h_i$.

Eq 3.1 can be solved using weighted sums of a radial basis function (RBF) (see Figure 3-3). Common choices for RBF include the following (but not limited to):

1. Linear: $\varphi(x) = x$
2. Thin-plate spline: $\varphi(x) = |x|^2 \log(|x|)$.
3. Triharmonic: $\varphi(x) = x^3$

Using the appropriate RFB function, in our case we found as most appropriate the triharmonic, we can then express the interpolation function as:

$$f(x) = \sum_{j=1}^n d_j \varphi(x - c_j) + P(x) \quad \text{Eq 3.2}$$

In the above equation, c_j are the locations of the constraints, the d_j are the weights, and $P(x)$ is a degree one polynomial that accounts for the linear and constant portions of f . Because the thin-plate radial basis function naturally minimizes Eq 3.1, determining the weights d_j , and the coefficients of $P(x)$ so that the interpolation constraints are satisfied will yield the desired solution that minimizes Eq 3.2 subject to the constraints. To solve for the set of d_j that will satisfy the interpolation constraints $h_i = f(c_i)$, we can substitute the right side of Eq 3.2 for $f(c_i)$, which gives:

$$h_i = \sum_{j=1}^k d_j \varphi(c_i - c_j) + P(c_i) \quad \text{Eq 3.3}$$

Since this equation is linear with respect to the unknowns, d_j and the coefficients of $P(x)$, it can be formulated as linear system. For interpolation in 3D, let $c_i = (c_i^x, c_i^y, c_i^z)$ and let $\varphi_{ij} = \varphi(c_i - c_j)$. Then this linear system can be written as follows:

$$\begin{bmatrix} \varphi_{11} & \varphi_{12} & \cdots & \varphi_{1k} & 1 & c_1^x & c_1^y & c_1^z \\ \varphi_{21} & \varphi_{22} & \cdots & \varphi_{2k} & 1 & c_2^x & c_2^y & c_2^z \\ \vdots & \vdots & & \vdots & \vdots & \vdots & \vdots & \vdots \\ \varphi_{k1} & \varphi_{k1} & \cdots & \varphi_{kk} & 1 & c_k^x & c_k^y & c_k^z \\ 1 & 1 & \cdots & 1 & 0 & 0 & 0 & 0 \\ c_1^x & c_2^x & \cdots & c_k^x & 0 & 0 & 0 & 0 \\ c_1^y & c_2^y & \cdots & c_k^y & 0 & 0 & 0 & 0 \\ c_1^z & c_2^z & \cdots & c_k^z & 0 & 0 & 0 & 0 \end{bmatrix} \begin{bmatrix} d_1 \\ d_2 \\ \vdots \\ d_k \\ p_0 \\ p_1 \\ p_2 \\ p_3 \end{bmatrix} = \begin{bmatrix} h_1 \\ h_2 \\ \vdots \\ h_k \\ 0 \\ 0 \\ 0 \\ 0 \end{bmatrix} \quad \text{Eq 3.4}$$

The above system is symmetric and positive semi-definite. So there will always be a unique solution for the d_j and p_j . The above system can be solved directly with the symmetric LU decomposition as long as the number of constraints are limited to a few thousand. In this work we used symmetric the LU decomposition from [NuRec93] to solve this system.

3.2.1.2 Prepare constrains for 2D input contours

We can create smooth functions for a given 2D or 3D shape using implicit functions. Our interest is the use of 2D planar contours as input and to generate a smooth 3D shape as output. We aim to fit an implicit function to a surface where all points lying on surface will satisfy the equation:

$$f(c_i^x, c_i^y, c_i^z) = 0 \quad \text{Eq 3.5}$$

In order to avoid the trivial solution that F is zero everywhere the off-surface points are appended to the input data and are given non-zero values, revising the interpolation problem:

$$f(c_i^x, c_i^y, c_i^z) = 0, \quad i=1\dots, n \quad (\text{for on-surface points})$$

$$f(c_i^x, c_i^y, c_i^z) = h_i, \quad i=n+1\dots, N \quad (\text{for off-surface points})$$

The boundary constraints are refer to the on-surface points. The question now comes how to generate the off-surface points. Since in this approach we use closed planar 2D curves we have to specify the number of points that should be interior and exterior to the curve. Paired with each boundary constraint is a normal constraint, which is a location at which the implicit function is required to take any non-zero positive and negative value (off-surface points). The locations of the normal constraints should be towards the interior of the desired curve, and the line passing through the normal constraint and its paired boundary constraint should be parallel to the desired normal to the curve. The function that is returned is an implicit function that describes our curve and the interpolation curve

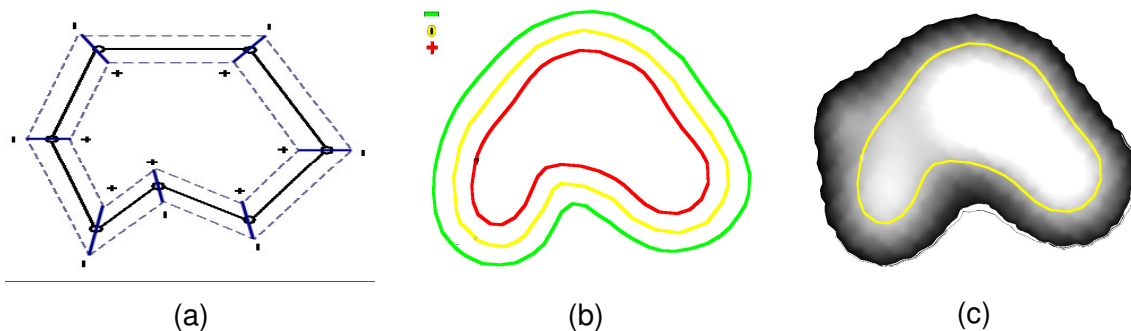


Figure 3-4. Extraction of normal constraints from the original contour (a). The off-surface points have the form of closed contours. They are generated along the contour normals and are indicated with plus and minus symbols. In (b) a manual generated (middle yellow line) and its normal constraints interior and exterior from the contour

will exactly pass through our boundary constraints.

Seven pairs of constraints are illustrated in Figure 3-4(a), with the boundary constraints shown as circles and the normal constraints as plus/minus signs. When we invoke implicit function interpolation with such constraints, the result is a function that takes on the value of zero exactly at our zero-value constraints and that is positive in the direction of our normal constraints (towards the interior of the shape). The closed curve passing through the zero-value constraints in Figure 3-4(c) is the iso-contour of the implicit function created using as input constraints those from Figure 3-4(b). Given enough suitably placed boundary constraints we can define any closed shape.

We now turn our attention to defining boundary and normal constraints for a given 2D shape. Assume that a given shape is represented as a gray-scale image. White pixels represent the interior of a shape, black pixels will be outside the shape, and pixels with intermediate gray values lie on the boundary of the shape. Let m be the middle gray value of our image's gray scale range. Our goal is to create constraints between any two adjacent pixels where one pixel's value is less than m and the other's value is greater. Identifying these locations is the 2D analogue of finding the vertex locations in a 3D marching cubes algorithm [Loren87].

The grey-scale image can be generated on different level, where contours have to get extracted, using predefined regular spaced grid. Each grid corner is a point (x, y, z) lying on the plane of the current level. To evaluate each corner the coefficients calculated from Eq 3.4 used. Thus, each point of the grid is substituted with the corresponding function value. Due to the nature of the implicit function shape, it is expected that at those levels where contour shape is about to be extracted grid edges will be marked with positive and negative values. To extract the contours, we try first to detect any edge in the grid whose end points being of opposite signs as shown in Figure 3-5. The opposite signs in the grid cell implies that in-between the cell edges there will be a point where the function can be evaluated and will result to zero value. Binary sectioning over the edge is used to localize the position of this value. After having this original point (shown as red square in Figure 3-5), the algorithm jumps to the positive corner and continues scanning the corners clockwise until a corner with opposite signed is found. We traverse the entire grid of each level until the contour is closed, visiting each grid cell that contains edges with opposite signs. The algorithm is capable to detect and extract more than one contour on a level.

3.2.1.3 Surface Reconstruction from Parallel Contours

In this chapter, we do not aim to present and compare the implicit surface reconstruction scheme with existing methods. Instead, we present a workflow on how to use the implicit functions interpolation as a tool for defining anatomical volumes from 3D data. The first type of problem we attempt to solve using implicit function interpolation is the reconstruction of 3D objects from parallel contours. Linear interpolation between key slices is a very common approach used in RTP process to accelerate target volume definition. Almost all contour interpolation methods consider only pairs of contours at any one time [Boiss88], [Payne94], [Bajaj95], and thus suffer from such normal discontinuities at the planes of the original slices. In the plane of slice z , the surface created between slice pairs $i-1$ and z will usually not agree in surface normal with the surface created between slices z and $i+1$.

To avoid discontinuities in surface normal, we must use information that involves more than just two slices at a given time. We can accomplish this using a generalization of the implicit function interpolation approach. Assume that we begin with k sets of constraints, one set for each 2D data slice. Instead of considering the contours in pairs, we place the constraints for all of the k slices into 3D simultaneously. Specifically, the constraints of slices i are placed in the plane $z = si$, where s is the spacing between planes. Once the constraints from all slices have been placed in 3D, we invoke the implicit function interpolation once to create a single implicit function in 3D for the complete set of contours. The zero-valued iso-surface exactly passes through each contour of the data. Due to the smooth nature of implicit function interpolation, the gradient of the implicit function is everywhere continuous. This means that surface normal discontinuities are rare, appearing in pathological situations when the gradient vanishes such as when two features just barely touch.

The contour interpolation result between parallel contours is illustrated in Figure 3-6. The kidney surface reconstructed in Figure 3-6(b) is a product of well-known reconstruction method from [Geige93]. The method used ten contours as input and produced near

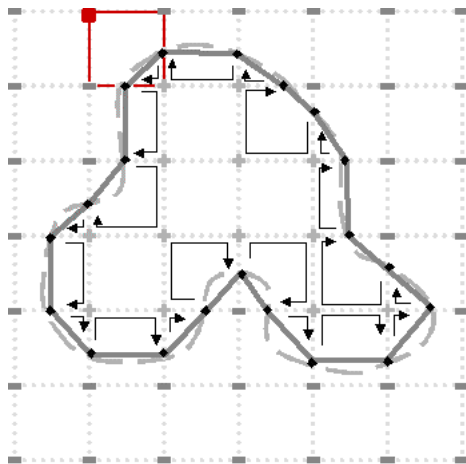


Figure 3-5. Contour tracing on a grid (single level) after evaluating the implicit function on each grid edge. The red arrow indicates the starting point of the algorithm

to 600 triangles. In Figure 3-6(c) the implicit function, interpolation is used to produce a mesh out of 19000 triangles. To extract the mesh for the implicit function we used the polygonizer proposed from Bloomenthal et. al. [Bloom94][Bloom97]. During the parallel and non-parallel contour constrain generation the contour spacing used in all of our results corresponds to the real contour spacing according to the acquired voxels size from the CT images. The contour spacing is an important control parameter for the implicit surface result. If the distance is small, only pairs of features from the two shapes that are very close to each other will be preserved through all the intermediate shapes. If the separation distance is large, the intermediate shape is guided by more global properties of the two shapes. In some sense, the separating distance specifies whether the shape transformation is local or global in nature.

The results illustrate that implicit surface reconstruction produces much smoother results than conventional triangulation algorithms. To achieve similar mesh quality with conventional triangulation methods larger amount of input planar contours and point samples are required. A very interesting and useful side benefit of using the implicit function interpolation method is that it produces smoothly rounded caps on the ends of surfaces, which is a very acceptable and suitable effect for describing anatomical structures.

Notice that in Figure 3-6(c) the reconstructed surface extends beyond the last contour constraints in the positive and negative z direction (the direction of slice stacking). This “hemispherical” component at the end of the stack is a natural side effect of the implicit function, and need not to be explicitly specified. This effect can improve organ shape rep-

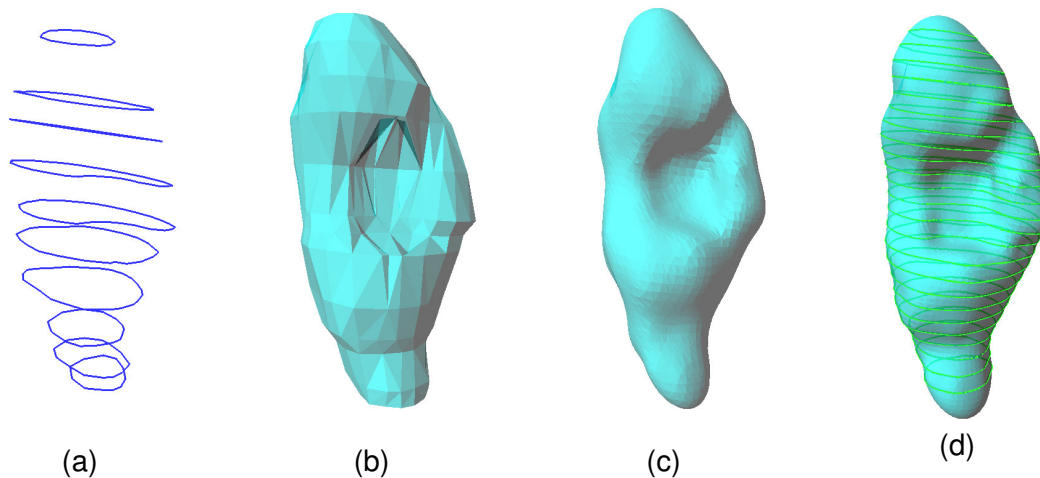


Figure 3-6. Reconstruction of kidney surface from parallel contours. In (a) eleven manual segmented contours have been used as input to the NUAGES polygon reconstruction algorithm (b) and in the implicit surface interpolation algorithm (c). In addition implicit contours have been extracted and using the contour tracing algorithm and reconstructed with the implicit surface.

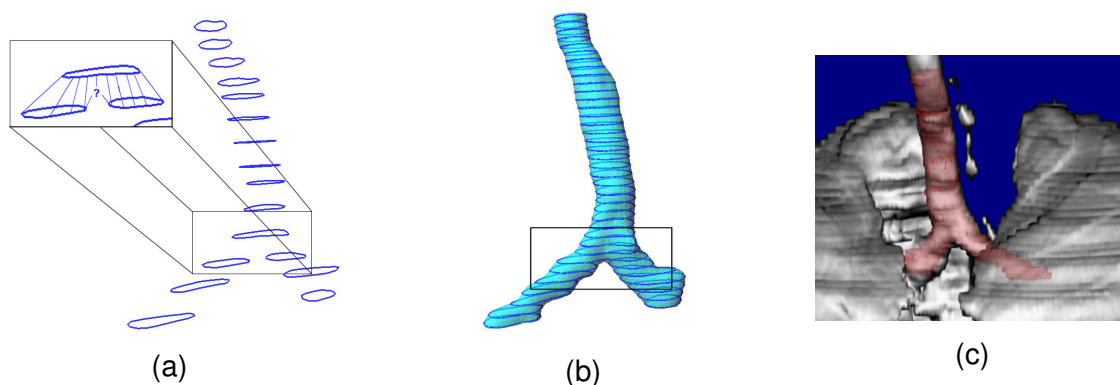


Figure 3-7. Contour samples defined according to trachea shape (a). In (b) the 3D surface reconstruction of the trachea shape using implicit surface interpolation. The extracted axial implicit contours have been used to allocate voxel grid reconstructed with red in (c), for comparison with the direct surface volume rendering.

resentation and in addition can reduce the number of contours needed for organ representation.

Reconstruction of organs with branches is a common issue in RTP. The common cases are the bronchial tree, prostate seminal vesicles, neck regions and immune system branches. In those cases, the user has to define a bigger amount of planar contours. Omitting key contours between single contour shapes and spited contours is usually not a options since advanced interpolation methods are required to feel the missing gaps. In a similar category belong key contours with concave that have to be interpolated with convex contour shapes. As shown in Figure 3-6 the kidney concave cavity can be represented very well using implicit surfaces in comparison to the standard contour-by-contour triangulation algorithm that lead to unreasonable triangle connections. For branching contour interpolation, it is usually difficult to decide a reasonable triangular connection rule,

when and where contours in a slice should be intersected or not. In Figure 3-7(a), an example is given where a number of contours describe the shape of the trachea. The main challenge for the contour interpolation of surface reconstruction algorithm is how to handle the bifurcation problem.

For the implicit surfaces, the definition of bifurcation is a property that can be handled with flexibility. The degree of bifurcation is highly related to the continuity degree of the implicit functions and to the distance between the single and contour pairs. As previously mentioned for contour distances we use the physical units as given from the CT volume data. The surface rounding-off presented in previous examples, is an effect not always useful. In this particular case round of the end of the branches is not needed. This feature can be controlled using a bounding box, applied during implicit function polygonization. In most of our examples the bifurcation approximation of the implicit surface fits very well with the natural bifurcation of the trachea (see Figure 3-7(c)).

3.2.1.4 Non-Parallel Contours

In the previous section, we only considered placing constraints within planes that are all parallel to one another. In this work the most powerful advantage provided from the implicit function interpolation is the capability to interpolate constraints located in 3D space. In RTP but also other medical images MPR images are often used for navigation and diagnosis. Investigating anatomical structures in those images provides very often more information than the standard cross-section (axial) images. Probably the greatest advantage is that organ length and shape can be better appreciated. For example if one is looking for the length of the kidney through the axial slices then more than 20 slices with 5mm voxel thickness in z direction have to be investigated until the positive and negative z direction limit is found. In case of course the slice thickness is smaller then number of slices increases and even more slices has to be investigated. In the frame of 3D simulation, powerful and efficient segmentation tools must be present. Hence, we adapted a fully 3D manual contour definition for the organ and tumour segmentation with the help of the implicit function interpolation.

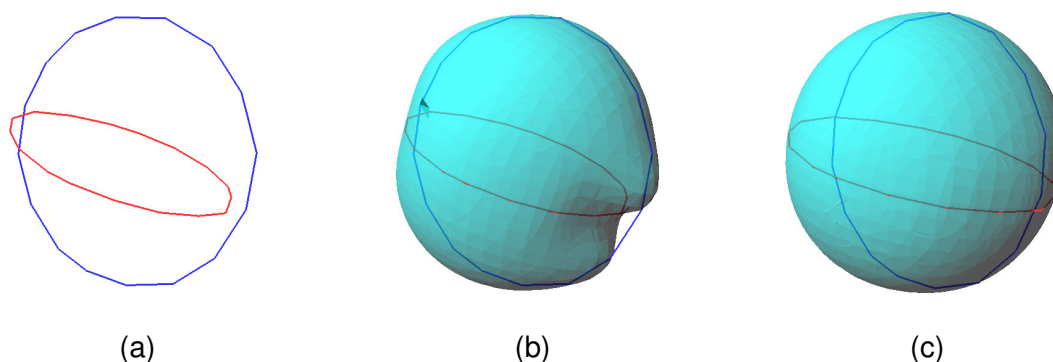


Figure 3-8. A simple surface reconstruction example from orthogonal contours.

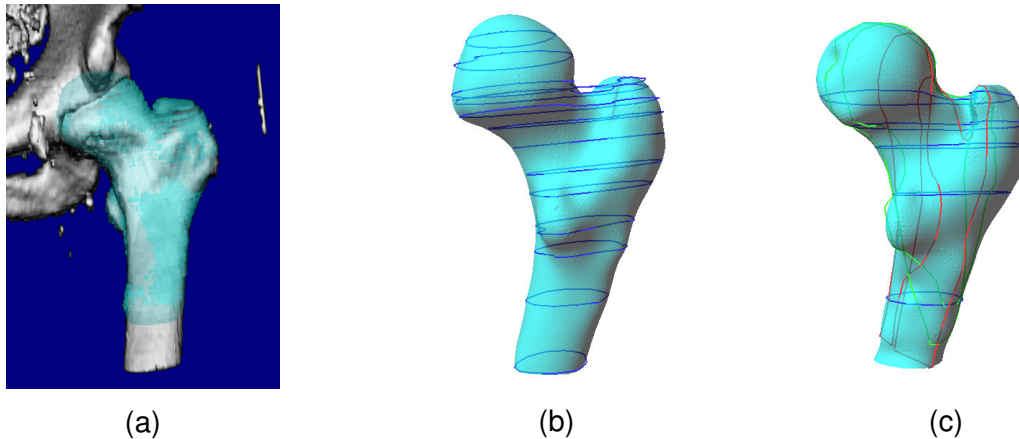


Figure 3-9. Surface reconstruction of a femur. In (a) the 3D volume reconstruction with the femur bone marked. In (b) an implicit surface reconstruction model of the femur using only parallel contours. In (c) a combination of different non-parallel contour and the final implicit surface of the femur.

To realize this concept the system allows the user to define closed planar contours on any of these planes. An even bigger degree of organ definition could be offered by allowing the segmentation of structures on any arbitrary cutting plane of the volume. The limitation of such approach will be the difficulty to orient the cutting plane in the volume. Definition of anatomical structures on the sagittal and coronal MPR images offers better description of the organ end shape providing more information than the axial contours. A common example is the round-off shape of organs, which is omitted when using axial planar contours as show in the previous example. However, this important detail must be included and taken into account for visualization and calculation purposes.

The most obvious problem one might face during non-parallel contour definition is the possibility to have different contour sizes. Usually anatomical structures in the MPR images have different appearance. This is due to image quality such as CT acquisition parameters, slice thickness and internal organ movements. During manual contour definition, it is often the case that the sagittal or the coronal contours have unequal slice length at the organ extremities. Considering this effect to the global surface shape we are about to reconstruct, it is rather less important. However, this problem becomes more noticeable when getting near those regions where the non-parallel contour constrains are close to each other (organ extremities) and the implicit function is forced to pass through all sample points.

In Figure 3-8(a) two orthogonal contours are generated with circular shapes. The coronal contour (red) has been designed smaller in diameter than the axial (blue). For those two contours we apply the implicit surface interpolation. Surface discontinuity is obvious in Figure 3-8(b) at the location where the coronal contour edge is far from the axial contour. This effect produces rapid changes on the final implicit surface shape since the implicit function will pass through every contour constrain. The way to solve this problem is by considering as reference the size of the bounding box of the first designed contour. The next contour designed from the user is forced to reach the size of the reference contour. To achieve this we apply a linear scaling on the second designed contour until the desired

contour size is reached and the contour edges are near to each other. The result of this approach is presented in Figure 3-8(c), where the size of the red contour is adjusted to the size of the blue contour. This is a rather simple example where only two contours are used. It is reasonable that in the clinical routine much more contours are used and the same problem will occur on several surface locations. The *contour scale matching* is omitted when the difference of the bounding box sizes is smaller than few millimetres (in our case 3mm). This can be an adjustable parameter from the user.

The implicit surface interpolation algorithm can be applied even if we consider a large number of contours in all three main planes. This will increase the number sample points and will make their topological relation among them more complex. As already mentioned defining structures on the sagittal and coronal reconstructions presumes that the image quality used is good enough to discriminate the necessary structures. The example Figure 3-9 illustrates the definition of the femur head, which is considered as a complex structure with a rather irregular concave shape. To reconstruct the femur shape using parallel contour (axial direction) we needed to place more than 13 contours Figure 3-9(b). The total area defined within the axial contours was 245.5 cm² and the number of sample points used was 315. For the same shape we needed to place 9 non-parallel contour as Figure 3-9(c) illustrates; five(5) axial, two(2) coronal and two(2) sagittal, which covered 282.3 cm² with number of sample point of 320. An example of non-parallel contour definition over the CT slices is given in Figure 3-10. Both implicit surface shapes have been reconstructed with small topological differences from the original shape. One can notice the difference of the femur head between the parallel and the non-parallel implicit surfaces.

An interesting issue to notice when reconstructing implicit surfaces from non-parallel contours is the inaccuracies of the surface at those points where contours from different direction are intersecting. From the algorithmic point of view this effect illustrates one important property of the implicit surface interpolation. On the other hand introduces topologic errors on the shape of the structure we attempt to reconstruct. To solve this problem we introduce the averaging of the two neighbour sample points. The result can replace the two ore more original sample points with a new one decreasing the surface inconsis-

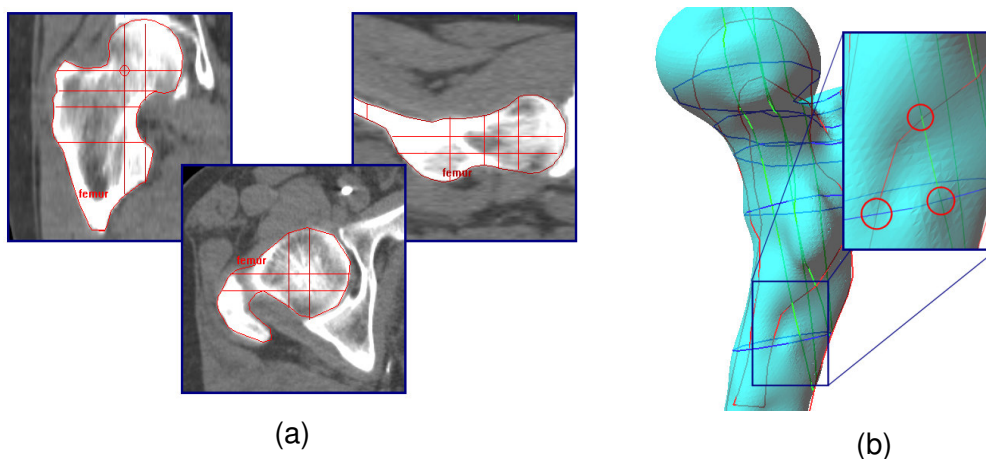


Figure 3-10. Definition of non-parallel contours on CT slices. In (a) from left to right: coronal, axial and sagittal contours. In (b) surface inconsistency at the intersection locations of the non-parallel contours.

tence. Probably the best way to prevent this effect is provide the necessary tools to the user in order to be able to adjust mismatches of the sample points interactively and also to be able to see the result in real time in 2D and 3D views.

The surface reconstruction of non-parallel contours can be applied to several organ type. There is nothing special about any particular set of planes once we are specifying constraints in 3D. We can mix together constraints that are taken from planes at any angle whatsoever, as long as we know the relative positions of the planes (and thus the constraints). Most contour interpolation procedures cannot integrate data taken from slices in several directions, but the implicit surface approach allows complete freedom in this regard. In the previous figures, all contours have been placed perpendicular to one another.

3.3 Segmentation of Normal Tissues

Several organs within the human body have very distinguishable characteristics, depending on the modality used to visualize them. In the frame of this work, we will focus on a specific organ the spine canal, which is of great importance for the workflow of the RT planning. In this work the base of the implemented segmentation, are the edge-detection techniques modified accordingly. All the segmentation algorithms have been applied and tested with CT images. However, they are not limited only to CT images, but they can also be used for segmenting MRI and US images. These techniques have been selected as optimum solutions between speed, effectiveness and complexity. It is well known that active contour and region base algorithms need from the user to pre-define conditions.

3.4 Segmentation of the spinal cord

The spinal canal is the anatomical region, which hosts the spine, one of the most vital organs in the human body. Its length starts from the base of the skull ending at the top of

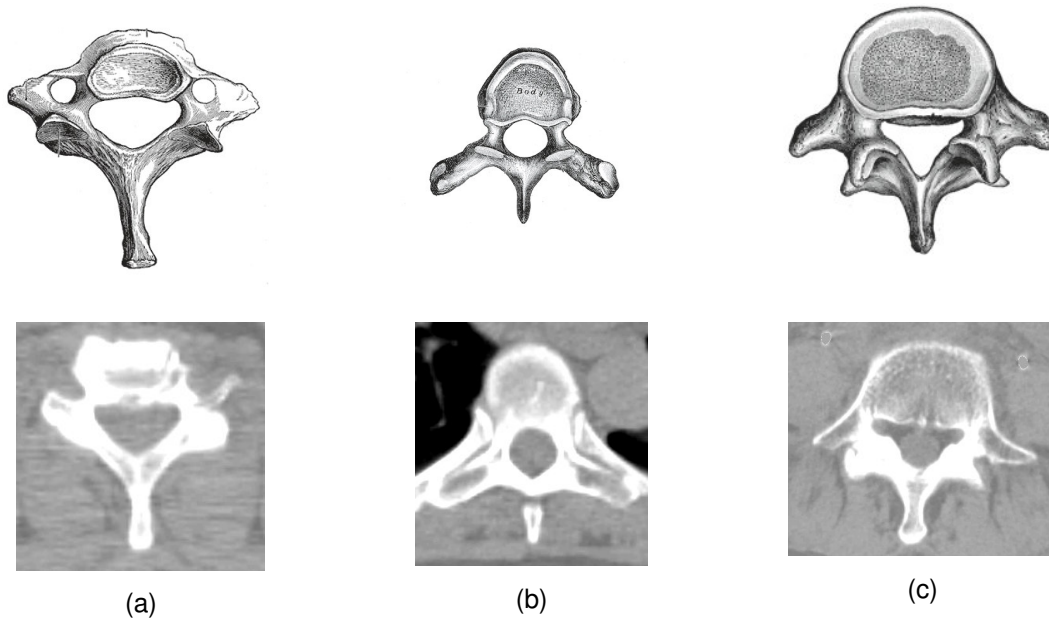


Figure 3-11. Illustration of different spinal cord vertebrae as anatomical sketches (top row) and as CT axial section (bottom row). In (a) a cervical vertebrae, in (b) thoracic and in (c) lumbar vertebrae.

the pelvic region. Spine is the channel of communication between the brain and the rest of the human body. Every signal transmitted from the brain follows the spine before the delivery to anatomical region. In radiation therapy it is very critical the accurate segmentation of the spine in order to calculate the allowed amount of dose during the treatment of the patient. The spinal canal is indicated as hole in the vertebrae with irregular ellipsoid and circular shapes, which in most cases are convex. Using CT imaging the contrast of the spine is very low compared with the surrounding tissues, which are mainly the bodies of the vertebrae.

Figure 3-12 illustrates several shapes of the spinal canal from different spine regions. The top row includes 3D sketches of vertebrae of the cervical, thoracic and lumbar level and the bottom row some axial CT images of the vertebrae in the corresponding levels respectively. Interesting to notice is that the spinal canal of the illustrated CT images is closed and well defined. This geometry can be segmented easily using image thresholding techniques. Nevertheless, except from the circular closed shapes, the spinal canal might be open, this happens at the locations where the vertebrae are joined, and the nerve tree distributes. Figure 3-12 illustrates such examples. At that region, the surrounding tissue contrast is very similar with the spine contrast and therefore any simple threshold segmentation technique like region-growing and edge tracking will fail.

In this section of the thesis, a new approach is described for the 3D segmentation of the spinal canal. The algorithm is a mixture of the edge detection combined with contour linear interpolation and a 2D radial ray-casting algorithm. The technique aims to detect the whole shape of the spinal canal with minimum user interaction. Main steps of the method are:

1. Definition of the starting point (User interaction)
2. Detection of the first sample contour using boundary tracking. Evaluate contours consistency (shape, location and texture)
3. Extract of the new starting point considering the centre of gravity of the current contour.
4. Propagation of the starting point to above and below cross sections from the original starting point

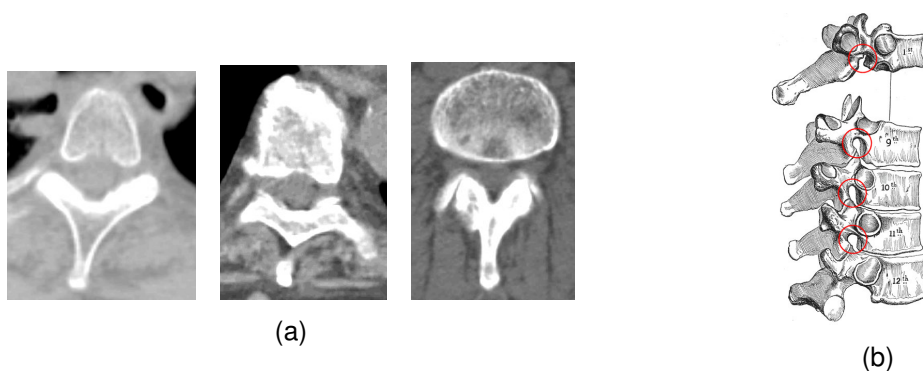


Figure 3-12. Discontinue spinal canal. In (a) three examples of CT images with open spinal canal. In (b), the red circles on the sketch indicate potential locations in the spine that will produce open vertebrae bodies when a CT acquisition will be made.

5. Repeat steps 2, 3 & 4 until all cross sections have been examined.

3.4.1 Definition of starting point

There are three choices one could have when attempting to define a starting point:

- a) Selection of a point inside a closed vertebra canal (see Figure 3-12)
- b) Selection of a point inside an open vertebra canal (see Figure 3-12)
- c) Selection of a point outside the vertebra body.

Selecting of a starting point as outside the vertebra point should result to a warning for the user that the algorithm cannot proceed with the spine tracing. To qualify such a case we use the HU range as an indicator. The selection of the starting point based on case a) is the optimal situation and the algorithm can proceed to the next step without any problem. If a starting point is defined inside an open vertebra then most likely the boundary-tracking algorithm will fail to continue. Due to the restrictions of the BT mentioned above, in this case it is not possible to initialize the tracing process from an arbitrary slice. Instead, a slice with closed vertebra's canal must be selected from the user. Due to this

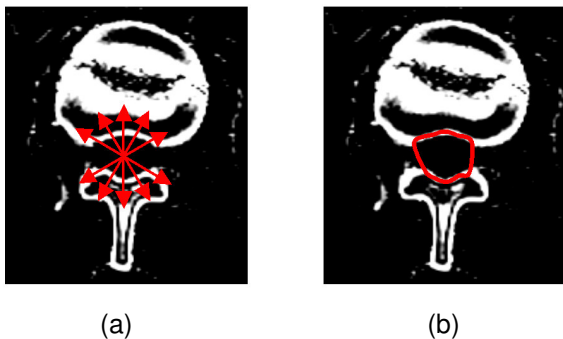


Figure 3-13. Angular tracing of open vertebra boundaries. In (a) the tracing of boundary points using angular scanning. In (b) the result contours after interpolating the original contours.

limitation the user must be trained under the trial-and-error principle until the wanted contour is found. As solution to this problem we developed an angular ray-casting (ARC) algorithm that enables the tracing of the vertebra location in an angular behavior using predefined values of angles (see Figure 3-13). This step is activated only if the BT fails to trace the spinal cord with a specific area and HU content of low range. The result of the ARC will be the generation of a number of points on the boundaries of the open vertebra. In order to generate the final contour shape we interpolate the traced points using the Spline approximation.

3.4.2 The Boundary-Tracking Algorithm

The key component of the method is the boundary-tracking (BT) algorithm [Haral85]. The implemented technique works on a 2D level and scans one CT image at a time. The CT image level corresponds to the original cross section image. The BT algorithm requires an initial point to start the tracing of the edge of the object under investigation. The initial point travels to one direction, vertical or horizontal until an edge of the investigated object is reached. In case the tracing point fails to reach the edge moving in one direction (e.g. vertical), the other one is used. This is repeated until the required edge is found.

Then the algorithm will start to investigate the surrounding pixel of that edge and check whether they belong to the current edge or not. This is done by selecting a range of HU

levels. The algorithm uses a constant threshold selection with levels [300 to 600] HU range. If the pixel under investigation is within the range then is classified as 1, otherwise as 0. Concurrently the classified pixels as 1 are stored in the memory with the detected sequence, recording the shape of the investigated organ. The edge detection algorithm has low complexity and therefore is quiet fast on processing. During the tracing process a large number of points is collected, and depending from the segmented area it might reach more than 300 sampled points. This has the benefit that every voxel detail is recorded providing high accuracy to the description of the contour shape. Alternatively, all these voxels enhance sharp edges giving an uncomfortable optical effect. Therefore, the original voxels are decimated to approximately 40% of the original number. Simultaneously the contour shape is also smoothed.

The main drawback of the BT is that is a binary approach and hence is very sensitive to grey value variations. If the threshold value is not selected properly then the system will fail to detect the appropriate canal shape. In case the algorithm slides from its edge path though a gap, then the algorithm will generate an overflow of points. To avoid this situation a maximum number of points is used as the limit. This can be very often the case when the vertebra's shape is interrupted from tumour metastasis or bone osteoporosis. Most of the inaccuracies of the segmentation method require the user intervention to optimise the result. An example of contour tracing using edge detection on single slice can be found in Figure 3-14. In image (a) an accurate edge detection of the spine. A misleading result of the algorithms due to boundary bridging is illustrated in image (b). Image (c) shows a completely erroneous segmented region. Instead of the spinal canal, the lower bony part of the vertebra is detected. To improve the algorithm performance we calculate a secondary volume map using the gradient estimators as described in [Levoy88]. This approach allows a comprehensive representation of tissue boundaries compared to the conventional thresholding techniques. The example in Figure 3-15 demonstrates how the boundary description can be improved using the gradient estimators.

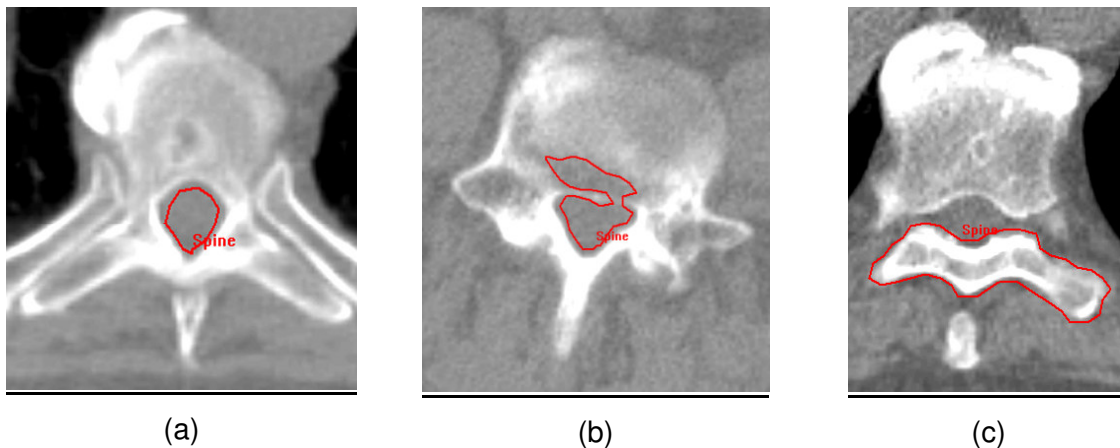


Figure 3-14. Spine boundary tracking of single slices. In (a) an accurate detection of the spine, in (b) a misleading detection of the spine due to osteoporosis and in (c) a failure of the BT algorithm due to open vertebra shape.

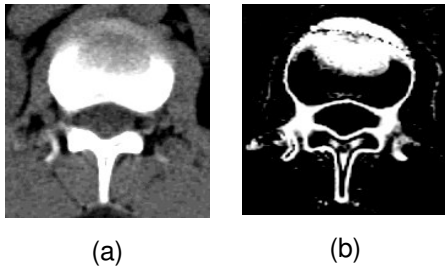


Figure 3-15. Difference between simple image thresholding (a) and gradient detection (b).

3.4.3 Tracing Conditions

After the user has defined the starting point, the edge detection algorithm is activated trying to specify the boundaries of the spinal canal. The threshold value we used for the segmentation has a range between from 50HU (inside spine) to 450HUs. This range of HU values might be slightly different among CT acquisition protocols. The edge detection algorithm is effective only in those cases where the shape of the canal describes a closed contour. If that is the case, the centre of gravity of the new

generated contour is calculated. If there are two starting points existing then they will be used to generate a straight line between them. The end of that line will propagate towards to the scanning direction within the CT volume. The intersection point with the next available cross section at the Z-direction will be used as starting point for the BT algorithms.

To segment the whole data volume we have to repeat the above step to both directions, left and right from the starting point. This process will generate automatically a virtual path that will reach even the last slice of the CT volume when this is necessary. During contour tracing some of the contours generated from the BT will be rejected due to incompatibility with the rest of the normal spine contours. The criteria used to qualify contours as belonging to the spine are:

- a) Contour area
- b) Distance of the centre of gravity of the current contour from the previous found.
- c) Texture value content.

Contours that do not fulfill the above properties will be deleted from the system and the system will continue searching and tracing contours on further cross sections. The deleted contours will be replaced with linear interpolated contours between. The contours found during BT will be used as the key contours for the linear interpolation algorithm.

To perform this, a slope factor **A** is calculated between the key slices. The value is

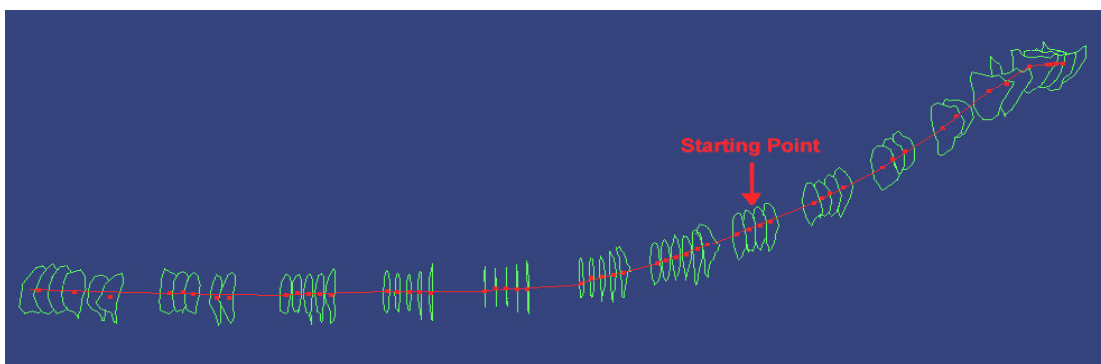
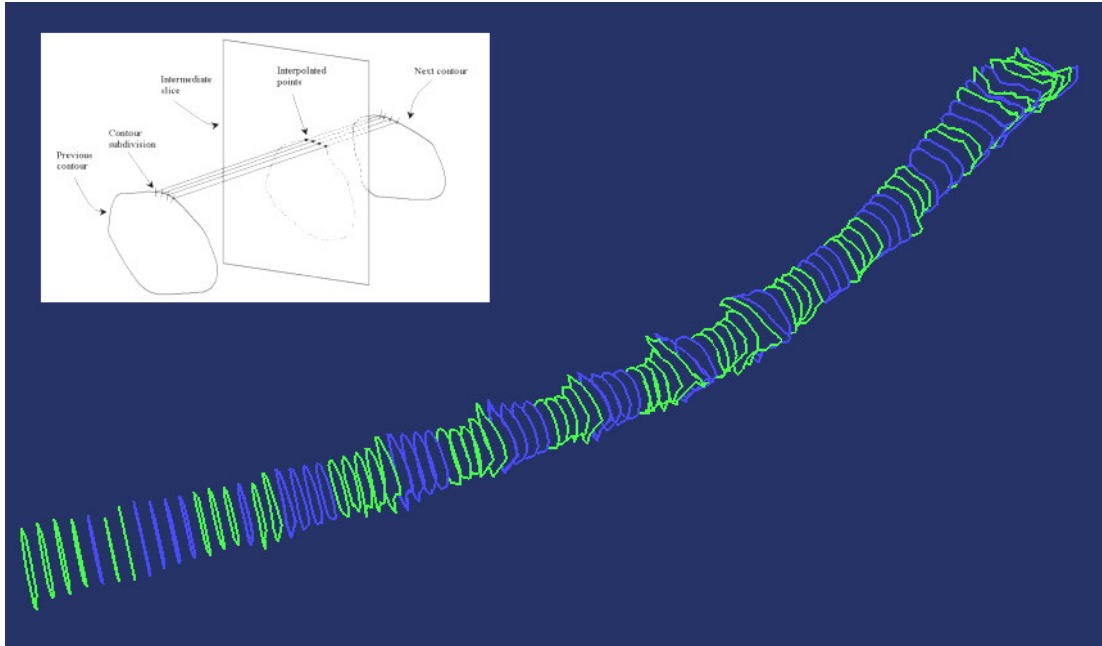
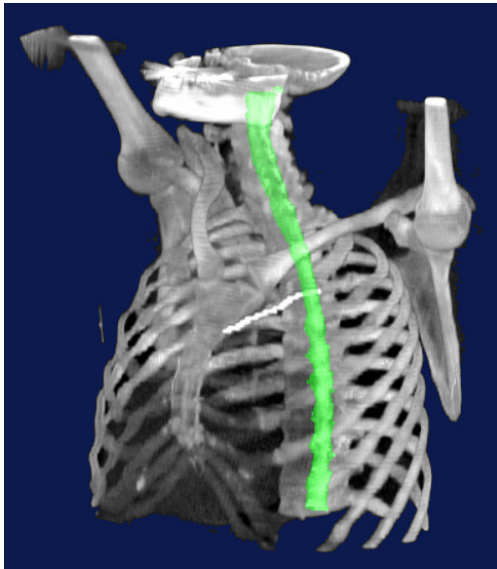


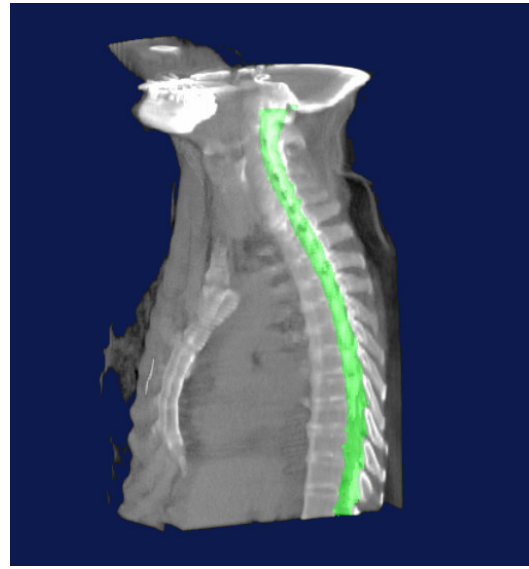
Figure 3-16. Wire loop display of the traced spine contours. The starting point is illustrated with an arrow. The sampling point path is drawn with the red line and the centre of gravity of each contour is shown using the red dot.



(a)



(b)



(c)

Figure 3-17. Linear interpolation between key contours. In (a) the principle of the linear contour interpolation is shown in the small image top left. In the spine shape the key contours are illustrated with green and the interpolated contours are illustrated with blue. Images (b) and (c) show spine segmentation results on CT data.

given by the equation:

$$A = \frac{(\text{Current_slice_pos} - \text{Previous_contour_pos})}{(\text{Previous_contour_pos} - \text{Next_contour_pos})} \quad \text{Eq 3.6}$$

Since each key contour has individual number of samples of segment points, the algorithm subdivides each contour into the same number of points in order to simplify the contour interpolation step. Then a starting point is selected, which is usually the point of the 12 o'clock position of the contour. To calculate the X and Y pixel (or voxel) position of the interpolated point we use the following formula:

$$X_{\text{int}} = X_{\text{previous_cnt}} + A * (X_{\text{next_cnt}} - X_{\text{previous_cnt}}) \quad \text{Eq 3.7}$$

$$Y_{\text{int}} = Y_{\text{previous_cnt}} + A * (Y_{\text{next_cnt}} - Y_{\text{previous_cnt}})$$

The principle and the result of the linear contour interpolation are shown in Figure 3-18 (a). Figure 3-19 (b) and (c) show spine segmentation results on CT data set.

3.4.4 Results

The algorithm was evaluated using 14 CT datasets from 14 arbitrary selected subjects. All subjects were scanned using spiral CT with equal slice thickness and space. Overall 1229 slices with 3mm thickness were collected. The segmentation accuracy was assessed by comparing the automatic computer-based segmentation, with the results obtained by manual analysis. Differences on the contour border on each slice level were assessed by computing the mean and RMS distance between the computer defined borders and the manually defined borders [Chala97]. In addition, the overall difference of the spinal cord volumes was assessed between the computers defined and the manually defined structures. These results are shown in Figure 3-18. The range of variation in volume meas-

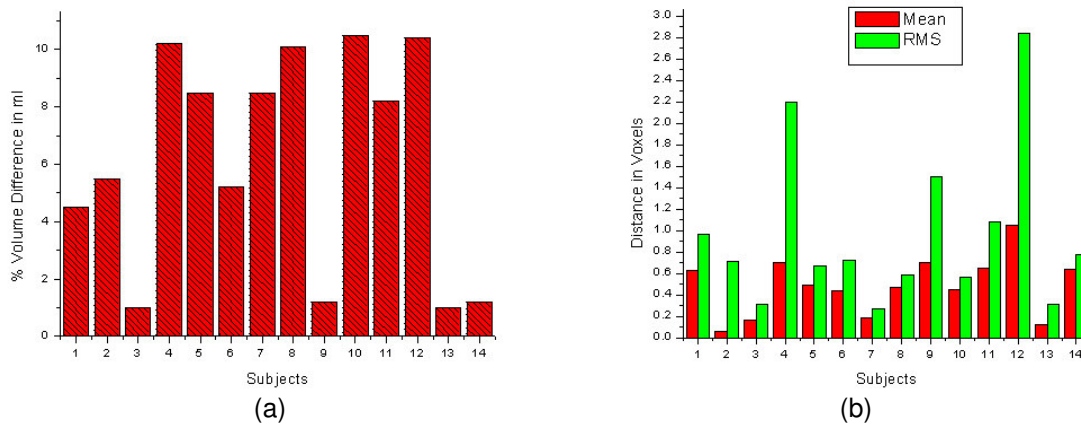


Figure 3-18. Comparison of manual and computer traced spinal cord contours. In (a) The percentage of volume difference in ml. In (b) Mean and RMS values between contour boundary distances.

urement was 1.0%-10.2%, with a mean variation of $6.14\% \pm 3.82\%$ (mean \pm standard deviation). The range of variation in boundary distance measurement was 0.05-1.05 in voxels, with a mean variation of 0.48 ± 0.27 . In addition the algorithm provides good speed performance since 1-2 seconds are needed in average in order to segment a volume with 90 slices on a Pentium III 933MHz processor.

3.5 Summary

In this chapter, we discussed a daily clinical problem in the frame of 3D Simulation and RTP; the definition of anatomical structures in CT data. We present a number of computer-based tools that can assist the segmentation process during the 3D simulation process. The methods presented here are categorized to manual and semi-automatic methods. For the manual volume definition, we present a 3D interpolation method based on implicit functions. Due to the high order of continuity of the function, the interpolation scheme can reconstruct a surface from 3D sample points that describes very accurately the shape of different anatomical structures. The input samples can be the product of contours defined on parallel imaging cross sections. Even more advanced is the capability of the algorithm to handle the non-parallel contours either perpendicular or even arbitrary placed relative to each other. This has been a new concept for radiotherapy imaging applications.

The conventional 2D segmentation tools on the axial cross sections have been for many years now the standard methods used. Advantages of the new concept is the flexibility and freedom given to the clinicians to investigate new ways of defining anatomical structures taking advantage of the full 3D information available on the multiplanar reconstructed slices such as sagittal and coronal, As a result the segmentation process improves in terms of speed and selectivity. In addition, the time needed to segment structures can be dramatically reduced since fewer contours are required to describe the shape of structures.

In this chapter, we also demonstrate that segmentation of the spinal cord can be achieved very accurately, in a few seconds with minimum user interaction; the user needs only to define an initial starting point for the algorithm. The algorithm can automatically trace the spine path through the complete volume of cross sections. False contours that are not correspond to the spine shape and position can be rejected automatically from the system and can be replaced with linear interpolated contours considering as key contours those already found by the system. The boundary-tracking methods used, belong to the deterministic approaches and therefore there is the tendency to produce misleading results under some circumstances. To reduce that effect data pre-processing and the gradient volume of the original CT data can be used as input to the segmentation routine.